Earth Syst. Dynam., 11, 673–695, 2020
https://doi.org/10.5194/esd-11-673-2020

Earth System Dynamics
Open Access
EGU

Climate engineering to mitigate the projected 21st-century terrestrial drying of the Americas: a direct comparison of carbon capture and sulfur injection

Yangyang Xu[1], Lei Lin[2], Simone Tilmes[3], Katherine Dagon[3], Lili Xia[4], Chenrui Diao[1], Wei Cheng[5], Zhili Wang[6], Isla Simpson[3], and Lorna Burnell[7]

[1]Department of Atmospheric Sciences, Texas A&M University, College Station, TX 77843, USA
[2]School of Atmospheric Sciences and Guangdong Province Key Laboratory for Climate Change and Natural Disaster Studies, Sun Yat-Sen University, Zhuhai, Guangdong, 519000, China
[3]Atmospheric Chemistry, Observations and Modeling Laboratory, National Center for Atmospheric Research, Boulder, CO, USA
[4]Department of Environmental Sciences, Rutgers University, New Brunswick, NJ, USA
[5]Mechanical and Aerospace Engineering, Cornell University, Ithaca, NY, USA
[6]State Key Laboratory of Severe Weather and Key Laboratory of Atmospheric Chemistry of CMA, Chinese Academy of Meteorological Sciences, Beijing, China
[7]School of Mathematical Sciences, University of Nottingham, UK

Correspondence: Yangyang Xu (yangyang.xu@tamu.edu), Lei Lin (linlei3@sysu.edu.cn)

Received: 2 January 2020 – Discussion started: 28 January 2020
Revised: 9 June 2020 – Accepted: 2 July 2020 – Published: 31 July 2020

Abstract. To mitigate the projected global warming in the 21st century, it is well-recognized that society needs to cut CO_2 emissions and other short-lived warming agents aggressively. However, to stabilize the climate at a warming level closer to the present day, such as the "well below 2 °C" aspiration in the Paris Agreement, a net-zero carbon emission by 2050 is still insufficient. The recent IPCC special report calls for a massive scheme to extract CO_2 directly from the atmosphere, in addition to decarbonization, to reach negative net emissions at the mid-century mark. Another ambitious proposal is solar-radiation-based geoengineering schemes, including injecting sulfur gas into the stratosphere. Despite being in public debate for years, these two leading geoengineering schemes have not been directly compared under a consistent analytical framework using global climate models.

Here we present the first explicit analysis of the hydroclimate impacts of these two geoengineering approaches using two recently available large-ensemble (>10 members) model experiments conducted by a family of state-of-the-art Earth system models. The CO_2-based mitigation simulation is designed to include both emission cuts and carbon capture. The solar-radiation-based mitigation simulation is designed to inject sulfur gas strategically at specified altitudes and latitudes and run a feedback control algorithm to avoid common problems previously identified such as the overcooling of the tropics and large-scale precipitation shifts.

Our analysis focuses on the projected aridity conditions over the Americas in the 21st century in detailed terms of the potential mitigation benefits, the temporal evolution, the spatial distribution (within North and South America), the relative efficiency, and the physical mechanisms. We show that sulfur injection, in contrast to previous notions of leading to excessive terrestrial drying (in terms of precipitation reduction) while offsetting the global mean greenhouse gas (GHG) warming, will instead mitigate the projected drying tendency under RCP8.5. The surface energy balance change induced by sulfur injection, in addition to the well-known response in temperature and precipitation, plays a crucial role in determining the overall terrestrial hydroclimate response.

Published by Copernicus Publications on behalf of the European Geosciences Union.

However, when normalized by the same amount of avoided global warming in these simulations, sulfur injection is less effective in curbing the worsening trend of regional land aridity in the Americas under RCP8.5 when compared with carbon capture. Temporally, the climate benefit of sulfur injection will emerge more quickly, even when both schemes are hypothetically started in the same year of 2020. Spatially, both schemes are effective in curbing the drying trend over North America. However, for South America, the sulfur injection scheme is particularly more effective for the sub-Amazon region (southern Brazil), while the carbon capture scheme is more effective for the Amazon region. We conclude that despite the apparent limitations (such as an inability to address ocean acidification) and potential side effects (such as changes to the ozone layer), innovative means of sulfur injection should continue to be explored as a potential low-cost option in the climate solution toolbox, complementing other mitigation approaches such as emission cuts and carbon capture (Cao et al., 2017). Our results demonstrate the urgent need for multi-model comparison studies and detailed regional assessments in other parts of the world.

1 Introduction

Mostly driven by CO_2 emissions and other greenhouse gas emissions, 21st-century global warming is one of the greatest crises facing the world today. A higher level of warming has been shown to lead to more frequent extreme weather and natural disasters (Schiermeier, 2011; Donat et al., 2013; Fischer and Knutti, 2015; Wang et al., 2017a; Lin et al., 2018), all having profound implications for public health, agriculture, and regional economies (Kunkel et al., 1999; Easterling et al., 2000; Knapp et al., 2008; Lesk et al., 2016). If left unchecked, temperature increases will soon pass the 1.5 and 2 °C warming levels (relative to the preindustrial era) in the coming decades and continue to rise (Peters et al., 2012), calling for a stronger need to comprehensively assess ecological and societal impacts at various warming levels and plan for adaptation at regional to local scales.

To mitigate future accelerated climate change, the importance of cutting CO_2 emissions and a few short-lived climate pollutants (SLCPs) has been well-recognized (Meinshausen et al., 2009; Shindell et al., 2012; Victor et al., 2015). But most recent analyses show that even with massive decarbonization to achieve a net-zero carbon emission by the mid-21st century, it is still not sufficient to stabilize global warming at a level relatively close to the present level (e.g., the 1.5 °C goal as proposed in the Paris Agreement) (Xu and Ramanathan, 2017; Miller et al., 2017). Instead, aggressive climate engineering schemes are needed in order to meet these low-warming targets (Keller et al., 2014; Tilmes et al., 2016; Lawrence et al., 2018). Among the many creative approaches (e.g., spraying seawater over the sea ice, Field et al., 2018; ocean fertilization, marine cloud brightening, and oceanic evaporation enhancement, Salter, 2002; and regional land albedo modification via vegetation or white roofs, Seneviratne et al., 2018), two schemes that can have a global impact have received the most considerable attention, leading to proof-of-concept technical designs (Vaughan and Lenton, 2011). The first is carbon capture and storage that directly extracts CO_2 from the atmosphere, especially close to its emission sources where the ambient concentration is high (Herzog, 2001). The second is sulfur injection into the stratosphere to reflect sunlight into space (Crutzen, 2006). Both approaches, especially the first one, can be expensive and at the same time could induce side effects, including those not yet identified. More scrutiny on the effectiveness and undesired consequences is thus urgently needed before any real-world deployment.

The utility of sulfur injection as a means to mitigate climate change has long been suggested (e.g., Crutzen 2006, Robock et al., 2009; Niemeier and Tilmes, 2017), but some potential drawbacks have also been identified (Pongratz et al., 2012; Keller et al., 2014; Effiong and Neitzel, 2016; Irvine et al., 2017; Helwegen et al., 2019). For example, a notable downside of sulfur injection (mostly designed to be initiated from the tropics to offset the higher intensity of solar radiation there) is that it tends to overcool the tropics while undercooling the polar regions due to the amplified greenhouse gas effect (Moore et al., 2014). To address these shortcomings, a strategic design has been proposed (MacMartin et al., 2017) to inject sulfur gas at multiple latitudes and selected heights to keep the north–south and pole-to-tropics temperature gradient largely fixed, while lowering the global mean temperature. With this design, global warming due to GHGs will be balanced in a more spatially uniform fashion. Following the initial success of numerical tests in Kravitz et al. (2017), Tilmes et al. (2018, BAMS) conducted a large-ensemble model experiment (Geoengineering Largen Ensembles, GLENS) under the same rationale. A large-ensemble approach is particularly useful to assess climate impacts because extreme weather can be better quantified with a larger sampling, and the role of natural variability internal to the climate system can be more robustly isolated.

Utilizing this GLENS dataset, recent studies have looked at hydroclimate change under this geoengineering method. Based on the analysis from Simpson et al. (2019), the precipitation in tropical and extratropical regions shows a dry-gets-wetter, wet-gets-drier pattern due to aerosol-induced stratospheric heating, opposite to the well-known pattern of

a dry-gets-drier response due to global warming. Cheng et al. (2019) also found that global land precipitation and evapotranspiration will be slightly reduced at the end of this century. Nevertheless, in both studies, the global soil moisture is well-maintained by the geoengineering method except in India and the Amazon. Cheng et al. (2019) explained that the reduction of summer soil moisture in India and the Amazon is dominated by a decrease in precipitation.

Our study extends the scope of the existing GLENS analysis by placing sulfur injection into the greater context of climate engineering (MacMartin et al., 2018). Here we aim to compare multiple metrics of the mitigation "benefits" of sulfur injection with carbon capture, another more expensive and yet more fundamental approach (e.g., to mitigate ocean acidification). Because many other analyses using GLENS have documented the global impact of sulfur injection, here we choose to focus on a smaller region of North and South America and on a specific set of land-based hydroclimate quantities that are of high relevance for agriculture, ecosystems, and socioeconomics indirectly related to the terrestrial carbon cycle in the Amazon and its feedback to climate change.

The structure of the paper is the following. In Sect. 2, we provide the details of the model description, experiment setup, the observational dataset used as model calibration, and the rationale for deriving climate benefits. In Sect. 3, we present and compare the climate benefits of two geoengineering approaches on a global scale. The regional changes are presented in Sect. 4 with detailed discussions on the mechanisms of the distinct results over the sub-Amazon and Amazon regions. In Sect. 5, we discuss the results of climate responses in terms of normalized changes with respect to global temperature change. Section 6 further discusses the implications and makes concluding remarks.

2 Methods

2.1 Global climate models

Two fully coupled ocean and atmospheric models, which are identical for the ocean and the tropospheric atmosphere component, are used in this study. The horizontal resolution of the atmosphere component for both models is set at $0.9° \times 1.25°$.

CESM1-CAM5 (the Community Earth System Model version 1 with Community Atmosphere Model version 5, shortened to CESM hereafter) is a global climate model that consists of coupled atmosphere, land, land ice, ocean, sea ice, and diagnostic biogeochemistry module component models, plus one coupler component. A new moist turbulence scheme explicitly simulates stratus–radiation–turbulence interactions, making it possible to simulate full aerosol indirect effects within stratus. A new shallow convection scheme uses a realistic plume dilution equation and closure that accurately simulate the spatial distribution of shallow convective activity. Computation of an updraft vertical velocity now allows for aerosol–cumulus interactions. The revised cloud macrophysics scheme provides a more transparent treatment of cloud processes and imposes full consistency between cloud fraction and cloud condensation. Stratiform microphysical processes are represented by a prognostic, two-moment formulation for cloud droplet and cloud ice, as well as liquid mass and number concentrations. The radiation scheme has been updated to the Rapid Radiative Transfer Method for GCMs (RRTMG) and employs an efficient and accurate correlated-k method for calculating radiative fluxes and heating rates. The three-mode modal aerosol scheme (MAM3) has been implemented and provides internally mixed representations of number concentrations and mass for Aitken, accumulation, and coarse aerosol modes.

Sharing most of the features described above, CESM1-WACCM (the Community Earth System Model version 1 with the Whole Atmosphere Community Climate Model, shortened to WACCM hereinafter) is a chemistry–climate model of the Earth's atmosphere from the surface to the lower thermosphere. A finite-volume dynamical core (Lin, 2004) is used for the tracer advection. The vertical resolution ranges from 1 to 2 km over the lower stratosphere and the tropopause. The land model CLM4.5 has fixed distributions of vegetation including interactive carbon and nitrogen cycles. CLM4.5 allows leaf area indexes to respond to climate changes. The Ball–Berry stomatal conductance model was utilized. The stomatal conductance is directly influenced by the relative humidity at the leaf surface, the CO_2 concentration at the leaf surface, and the soil water.

The major difference between WACCM and CESM is the stratospheric atmosphere component. WACCM has a high-top configuration that extends to about 140 km (6×10^{-6} hPa) and has a comprehensive representation of stratospheric chemical and dynamic processes (Mills et al., 2017), both crucial to simulate the radiative impact of stratospheric aerosols (via volcanic or artificial injection). The sulfur injection large-ensemble simulation is only available in the WACCM version. CESM has a typical model top at around 40 km, and the CO_2 mitigation large-ensemble simulation is only available in this model version.

Note that the model structural differences here can affect simulated climate response. The climate sensitivity is 4.1 K under a doubling of CO_2 for CESM and 5.2 K for WACCM (similar to a new version recently released; Gettelman et al., 2019). Both are within the CMIP5 range and are more in line with the higher CMIP6 range. Additionally, the land components are also different between these two versions due to incremental model development. CESM used an earlier version of CLM4 and WACCM used an updated version of CLM4.5. According to Cheng et al. (2019), relative to the earlier version CLM4, CLM4.5 includes modifications of the hydraulic properties of frozen soils and thus some seasonal changes in Arctic temperature. In the following analysis, we made attempts to address the caveat of model differences by (a) applying corresponding bias corrections to future climate re-

sponse simulated by these two models separately (Sect. 2.5) and (b) normalizing the response with respect to the temperature response (Sect. 5).

2.2 Numerical experiments

Two pairs of model simulations were conducted and published in the last few years, both featuring a large ensemble to enhance the robustness of examined climate responses, especially at a regional level. The WACCM set (http://www.cesm.ucar.edu/projects/community-projects/GLENS/, last access: 27 July 2020) is aimed at stabilizing the climate at its 2020 level with sulfur injection. The CESM set (low warming large ensemble; http://www.cesm.ucar.edu/experiments/1.5-2.0-targets.html, last access: 27 July 2020) is aimed at climate stabilization at 1.5 and 2 °C warming levels, with aggressive emission cuts and rapid growth of negative emission technology, an extreme mitigation scenario. Land cover and land use in these two pairs of simulations are consistently the same as in RCP8.5.

With the two sets of paired simulations, the effect of the two geoengineering approaches can be assessed by contrasting the run with geoengineering applied with the baseline potential warming worlds, which we would refer to as the climate benefits. Of course, for specific regions and certain climate variables, it may turn out that the climate benefits are negligible or even negative; i.e., geoengineering makes climate change under RCP8.5 even worse.

Stratospheric sulfur injection

The simulations were conducted with WACCM: one with baseline emissions (RCP8.5) and the other with sulfur injection applied at 2020 and afterward (hereafter referred to as sulfur injection). The amount and location of sulfur injection were strategically selected to stabilize the temperature at the present-day level and minimize undesired perturbation to the latitudinal temperature gradient (Tilmes et al., 2018). The simulation was repeated multiple times (see Table 1 for details) to form a larger ensemble (Geoengineering Large ENSemble, GLENS; Tilmes et al., 2018), which enhances the statistical significance of the assessed climate impact, especially at a regional level.

Carbon capture

Similarly, two simulations were conducted with CESM: one with baseline emissions (RCP8.5) and the other with CO_2 removal and emission cuts applied to start in 2015–2020 (hereafter referred to simply as carbon capture). This scenario is constructed to be a much more aggressive decarbonization pathway than RCP2.6 (see details in Sanderson et al., 2017). Net-zero carbon emission is thus reached at 2050, beyond which the net emission turns negative, which helps the planet to stabilize at the 1.5 °C warming level, just slightly higher than the present-day (2010–2019) temperature level. We show the mass amount of CO_2 reduction (combining emission cuts and various forms of net emission technology) and the associated negative radiative forcing in Fig. 4 to illustrate the idealized trajectories and to compare with well-studied RCP2.6. However, the technical feasibility and required socioeconomic shift to facilitate the scale-up of capacities such as direct air capture and clean energy transition (Hanna et al., 2020) are beyond the discussion in this paper.

2.3 Hydroclimate variables examined

In this study, we focus on climate quantities over land due to their high relevance for agriculture, ecosystems, and the carbon cycle, including the following.

a. T: surface air temperature at the reference height of 2 m above the ground.

b. P: total precipitation, which includes rainfall and snowfall without differentiating large-scale or convective components as formulated in the model.

c. PET: potential evapotranspiration, which represents the atmospheric demand for water. PET is calculated using model output, following the physically based Penman–Monteith equation (Shuttleworth, 1993), which includes key parameters of surface air temperature, surface-available energy, surface wind speed, and relative humidity.

d. Aridity index (P / PET): calculated as the simple ratio of annual P and annual PET (Mortimore et al., 2009; Hulme, 1996; Middleton and Thomas, 1992). P / PET is highly correlated with vegetation types (Feng and Fu, 2013; Huang et al., 2017). Using the P / PET classification by the United Nations Convention to Combat Desertification (United Nations Convention to Combat Desertification, 1994), drylands (characterized by P / PET <0.65) are further classified into various types, including subhumid ($0.5 < P$ / PET <0.65), semiarid ($0.2 < P$ / PET <0.5), arid ($0.05 < P$ / PET <0.2), and hyperarid (P / PET <0.05).

e. Other variables to depict aridity and corroborate the aridity index.

To further test the utility of P / PET as a metric to depict aridity conditions, we show the similar temporal evolution of P / PET with soil moisture and that between PET and actual ET (another metric commonly used) over major land regions (60° S to 60° N) in Fig. 1. Spatial patterns also show similar agreement between P / PET and soil moisture as well as PET (another metric commonly used) for both present-day and future change (Fig. 2), again supporting the appropriateness of using P / PET as an aridity metric.

Table 1. The model experiments.

Experiment short name	Model	Simulation period	Ensemble size	Reference
CESM_Historical	CESM1-CAM5	1975–2005	30	Kay et al. (2015)
CESM_RCP8.5	CESM1-CAM5	2006–2099	30	Kay et al. (2015)
CESM_CarbonCapture	CESM1-CAM5	2006–2099	10	Sanderson et al. (2017)
WACCM_RCP8.5	CESM1-WACCM	2010–2099	20 before 2030, 3 after 2030	Tilmes et al. (2018)
WACCM_SulfurInjection	CESM1-WACCM	2020–2099	20	Tilmes et al. (2018)

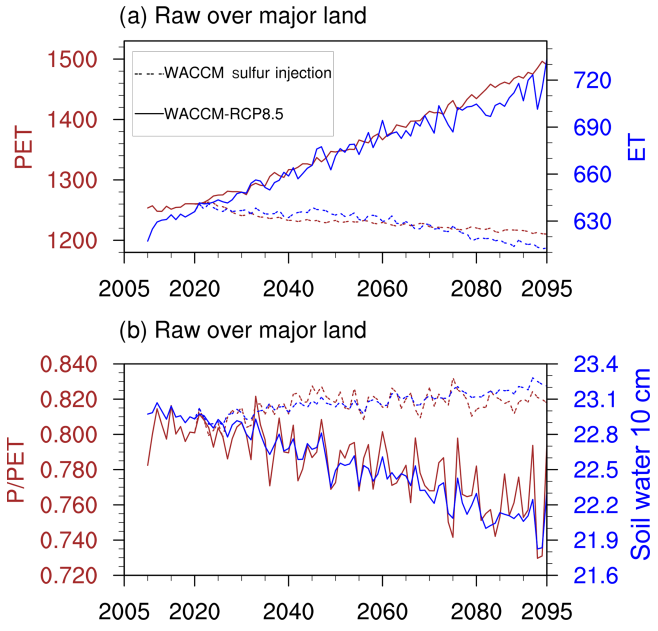

Figure 1. **(a)** PET (mm yr^{-1}) and ET (mm yr^{-1}) as simulated by WACCM over global major land regions (60° S to 60° N) only because P / PET is not a good indicator of drought conditions over snow-covered cold regions. **(b)** P / PET (unitless) and soil water in the top 10 cm layer (mm). The solid lines are for the left y axis and the dashed lines are for the right y axis. Red lines are under RCP8.5 and blue lines are under sulfur injection. Note that no bias correction or smoothing was performed for this figure. CESM results are not shown because **(a)** there is no reduction of soil moisture in the RCP8.5 warming, and **(b)** there is no separation of soil moisture in the long-term trends between the RCP8.5 and mitigated warming simulations, presumably due to model deficiency outside the Americas because within the Americas (Fig. 2), the CESM results are largely consistent with WACCM.

2.4 Bias correction of the raw model results

Climate model output cannot be taken at its face value, especially for future projection. The analysis, especially regarding the future projection, must consider the potential model bias in simulating the past and the present as well as the uncertainty inherent to climate models that are so far poorly constrained. Considering these, we corrected the model-simulated T, P, and PET based on the observational dataset, following the approaches in Dai (2011) and Feng and Fu (2013). The NOAA Climate Prediction Center (CPC) data (Fan and van den Dool, 2008; Chen et al., 2002) is used as the benchmarking temperature and precipitation over land. The Global Land Data Assimilation System (GLDAS) (Rodell et al., 2004) provides the surface sensible heat flux and latent sensible heat flux, specific humidity, and wind speed to derive the observation-based PET as in Feng and Fu (2013). The climate variables over the ocean are not corrected and thus not analyzed in this study.

The bias correction based on the observational dataset is only directly applied to CESM_Historical (with 30 runs from 1975 to 2005). The bias correction will force the model output to agree with the observed 1975–2005 climatology (and remove the bias of the seasonal cycle if any) but not necessarily to agree with the observation every year. In a nutshell, the temperature is adjusted using the addition or subtraction of identified biases on a monthly basis. For P or PET, the variables are adjusted using multiplication or division of identified biases on a monthly basis. A multiplication or division is used instead of addition or subtraction to avoid negative numbers for P or PET. Note that the difference between WACCM_RCP8.5 and WACCM_SulfurInjection will yield the "impact" of sulfate injection. The impact will change compared to raw data without bias correction because, for precipitation and PET, the bias correction is done via multiplication or division and not simple addition or subtraction.

The same bias correction is applied to future simulations of CESM (CESM_RCP8.5 and CESM_CarbonCapture in 2006 and afterward), which branched from the CESM_Historical in 2005. For WACCM_RCP8.5 simulations, we indirectly adjust them to agree with the corrected CESM_RCP8.5 in 2010–2019 (the "present day"). We could not adjust WACCM directly based on observations because the WACCM_RCP8.5 simulation only starts in 2010 and overlaps the observation record (ending in 2019) for less than 10 years. Similarly, WACCM_SulfurInjection was adjusted to match WACCM_RCP8.5 in 2020 (when it branches from WACCM_RCP8.5).

3 Global mitigation

3.1 Temperature

In Fig. 3, we show the long-term changes simulated by all four model experiments (two baseline worlds and two mitigated climates via different geoengineering schemes). We focus on the following three periods: the present day (2010–2019), mid-century (2046–2055), and the end of the century (2086–2095). Without the bias correction, the models do not agree on T and P for the recent period of 2005–2020 (Fig. 3a–b; see also the regional map in Fig. 2, first row). Therefore, it is essential to apply the bias correction to model output before carrying out a meaningful comparison of future changes. For example, comparing Fig. 3b and d, WACCM appears to have a 25 % positive bias for precipitation over major land, and CESM has a smaller positive bias.

Comparing the bias-corrected model output (Fig. 3c and d), because of the larger climate sensitivity, WACCM warms up faster than CESM, reaching a 6 °C warming over land under RCP8.5 just within this century (T for 2086–2095 – T for 2010–2019), which is ∼ 7 °C relative to the preindustrial, thus posing an existential threat to mankind if it becomes a reality (Xu and Ramanathan, 2017). CESM, with a climate sensitivity of 4 °C, simulates a 4.7 °C warming over the major land areas during the 21st century. The two types of mitigation efforts, by design, would lead to a similar amount of temperature stabilization to a level close to the present day. The sulfur injection simulation here leads to a cooling of 6 °C towards the end of the century compared with the baseline warming. This larger cooling is designed to largely balance the projected warming by introducing a large amount of sulfur gas, some from locations off the tropics (Tilmes et al., 2017; Kravitz et al., 2013).

The mid-century warming over global major land projected by the two models amounts to 2.0 to 2.5 °C compared to the present day (Table 2). Sulfur injection can completely offset the warming by 2.4 °C, while carbon capture can only mask about 70 % (1.3 °C to 2.0 °C). Even though the carbon capture scheme is introduced slightly earlier in 2015 to 2020, the longer lifetime of CO_2 makes the impact of perturbation on the carbon cycle and atmospheric concentration slower to emerge (Fig. 4e vs. f) compared to sulfur injection. This additional inertia (or lag) in CO_2-emission-based mitigation is well-noted when the CO_2 emission cut was previously contrasted with the mitigation of short-lived climate pollutants (e.g., Hu et al., 2013). Towards the end of the century, the lagging effects in the carbon capture case become negligible, and both schemes can almost completely offset the projected warming in the baseline by 4.0 and 5.7 °C out of the 4.5 and 5.8 °C baseline warming, respectively (Table 2, column 1, right).

3.2 Precipitation

Similar lagging effects are also found for global land precipitation. Table 2 shows that the mid-century reduction due to carbon capture is 31 % of the projected increase (23.0 mm yr^{-1}), and sulfur injection can reduce the precipitation increase by as much as 75 %. Again, towards the end of the century, the difference between the two cases, in terms of potential mitigation benefits, becomes smaller (62 % reduction by carbon capture and 98 % by sulfur injection).

The close to 100 % reduction of precipitation increase due to sulfur injection is worth commenting on. Because of the lack of direct radiative heating in the troposphere because CO_2 or black carbon aerosols, sulfate aerosols will have a larger precipitation effect (per degree of global mean temperature change) compared to CO_2 (Lin et al., 2016, 2018). Another alternative perspective to explain the overdrying (or the slowdown of the hydrological cycle) due to geoengineering is the increase in atmospheric stability and suppressed evapotranspiration, especially in the tropics, which tends to be overcooled in previous sulfur injection model experiments. As a result, when the amount of sulfur injection is carefully adjusted to balance the CO_2 warming, total rainfall will usually be excessively suppressed (so-called overdrying) (e.g., Bala et al., 2008; Jones et al., 2013; Crook et al., 2015).

However, in this WACCM setup, the overdrying consequence, especially over the tropics, is dampened. This is likely due to the following reason. In the current experiment design, sulfur injection is more heavily introduced to the extratropical region and thus induces a much-reduced tropical overcooling compared to previous stratospheric geoengineering experiments. Indeed, the global mean temperature, as well as the north–south gradient, will be well-preserved while offsetting the baseline CO_2 warming. This relatively weaker tropical cooling (again, because of the larger forcing imposed off the tropics) leads to a smaller overdrying in terms of precipitation, despite a persistent suppression of large convective precipitation (Simpson et al. 2019). From Fig. 3d, sulfur injection will lead to a negligible decrease in precipitation by 4–6 mm yr^{-1} (WACCM_SulfurInjection: 2086–2095 vs. 2020–2029) over the majority of the land. The overdrying is stronger (12–15 mm yr^{-1}) if the model output is not bias-adjusted (Fig. 3b). This overdrying, despite being small in this model, is considered to be a side effect of sulfur injection and is often used as an argument against its deployment. In contrast, carbon capture falls short in offsetting the full magnitude of projected precipitation increases (green line in Fig. 3b, d) and thus will not run into the problem of overdrying.

The applicability of this precipitation-centered perspective in assessing terrestrial aridity will be put to the test in the next subsection.

Table 2. The changes in key hydroclimate variables (bias-corrected based on observation) over major land (60° S to 60° N). All numbers are derived from the time series in Fig. 3. All changes are statistically significant at the 95 % level. The definition of major land is the land regions over 60° S to 60° N, thus excluding cold regions where seasonal snow cover or a permanent ice sheet surface makes P / PET less useful as a predictor for aridity and vegetation types. The focused periods are the present day (2010–2019), mid-century (2046–2055), and the end of the century (2086–2095). The values in parentheses are percentages relative to present-day levels. The uncertainty estimate based on the large-ensemble spread (1 standard deviation) is after ±.

Variables	T (°C)		P (mm yr^{-1})		PET (mm yr^{-1})		P / PET (unitless)	
Time periods	Mid-century	End of century	Mid-century	End of century	Mid-century	End of century	Mid-century	End of century
Changes under RCP8.5 by CESM (percentage relative to present day)	2.0 ± 0.3	4.5 ± 0.3	23.0 ± 24.0 (2.9 ± 3.1 %)	59.2 ± 32.4 (7.6 ± 4.2 %)	93.2 ± 13.9 (7.5 ± 1.1 %)	229.1 ± 15.2 (18.5 ± 1.2 %)	−0.03 ± 0.02 (−4.2 ± 3.2 %)	−0.06 ± 0.02 (−9.2 ± 3.8 %)
Changes under RCP8.5 by WACCM (percentage relative to present day)	2.5 ± 0.3	5.8 ± 0.4	54.2 ± 40.5 (7.0 ± 5.2 %)	123.2 ± 57.9 (15.8 ± 7.4 %)	103.8 ± 14.5 (8.4 ± 1.2 %)	249.4 ± 14.6 (20.1 ± 1.2 %)	−0.01 ± 0.03 (−1.3 ± 5.3 %)	−0.02 ± 0.04 (−3.6 ± 6.3 %)
Carbon capture benefits (percentage relative to CESM_RCP8.5)	−1.3 ± 0.1	−4.0 ± 0.1	−7.1 ± 6.4 (−0.4 ± 0.8 %)	−36.8 ± 5.5 (−4.2 ± 0.7 %)	−55.4 ± 4.5 (−3.9 ± 0.4 %)	−188.8 ± 3.3 (−14.6 ± 0.3 %)	0.02 ± 0.01 (3.2 ± 1.1 %)	0.06 ± 0.01 (8.8 ± 0.9 %)
Sulfur injection benefits (percentage relative to WACCM_RCP8.5)	−2.4 ± 0.1	−5.7 ± 0.1	−40.4 ± 8.6 (−5.2 ± 1.1 %)	−121.0 ± 7.9 (−15.5 ± 1.0 %)	−128.0 ± 3.0 (−10.3 ± 0.2 %)	−289.5 ± 3.9 (−23.3 ± 0.3 %)	0.03 ± 0.01 (5.1 ± 1.1 %)	0.05 ± 0.01 (7.2 ± 1.2 %)

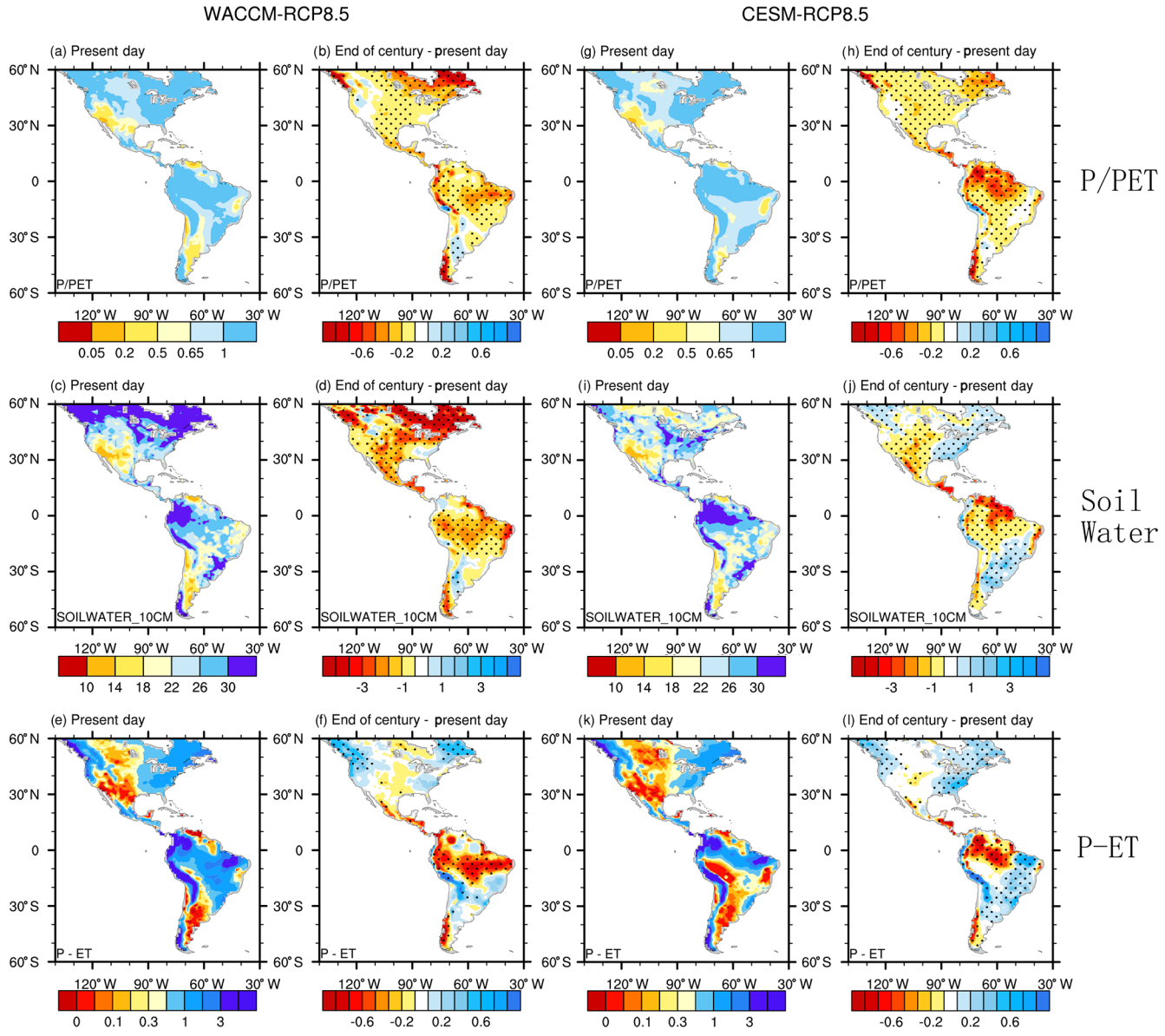

Figure 2. In the two left columns are WACCM-simulated P / PET (unitless), soil water (mm), and P-ET (mm d^{-1}) in the present day and at the end-of-century change under RCP8.5. The two right columns are the same as the left but for CESM. Note that all data here in Fig. 2 are without bias correction as in Fig. 1. The focused periods are the present day (2010–2019) and the end of the century (2086–2095). The areas with stippling in the panels labeled "End of century – present day" indicate where the differences are significant at a 95 % confidence level following a Student's T test. Similar results are presented in Fig. 5 but after bias correction and in relative terms (%).

3.3 PET and P / PET

It is increasingly well-recognized that precipitation alone does not reflect the full effects of the hydrological cycle on the terrestrial ecosystem. A full suite of aridity indices has been developed and is continuously being improved to provide a better depiction of aridity conditions (Mishra and Singh, 2010). It is beyond the scope of this paper, which emphasizes the contrast of two climate engineering schemes, to discuss the advantages and limitations of those approaches. However, we included more than one indicator from the model output to examine the robustness of our results largely based on P / PET. We showed that ET and soil moisture are closely correlated with PET and P / PET, respectively, over the global scale (Fig. 1). Moreover, Fig. 2 shows that there is broad agreement between P / PET, soil moisture, and P-ET not only for the present-day climatology but also for the future increase under the warming scenarios.

The major difference between the two geoengineering approaches, when viewed on a global scale, is due to PET. Despite an increase in P, the projected PET growth that ap-

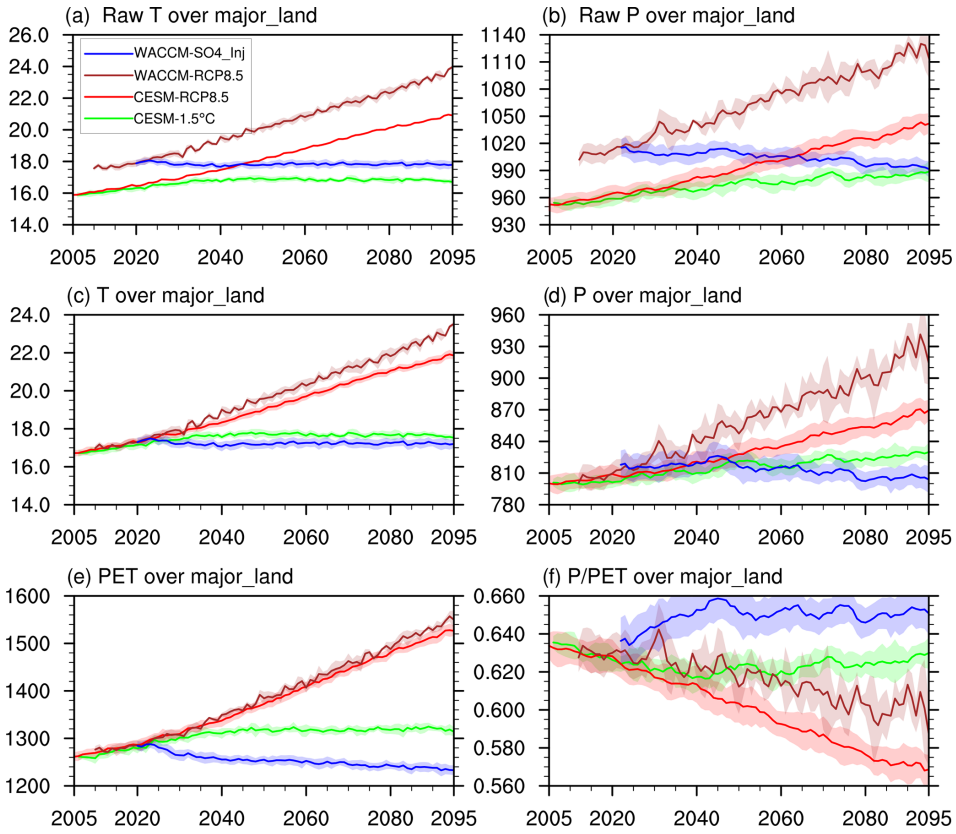

Figure 3. The annual average of major land temperature (T) (°C) (**a, b** without bias correction and **c, d** with bias correction) and major land precipitation (P) (mm yr^{-1}) (**a, b** without bias correction and **c, d** with bias correction). Panels **(e, f)** show the major land PET (mm yr^{-1}) and major land P / PET (unitless) (after bias correction). Shading represents the standard deviation of ensemble members. We have applied decadal smoothing to all the time series, but note that WACCM_RCP8.5 has three ensemble members during 2030–2099 and thus has large fluctuation due to natural variation in contrast with 10 or more ensemble members in other cases.

Table 3. Dryland area (millions of square kilometers) for semiarid and arid types. North America is 15–60° N and 230–300° E. South America is 60° S–10° N and 280–330° E.

Semiarid or arid area (km^2)	Global major land	North America	South America
CESM_Historical (after bias correction, 1975–2005)	20.4/15.0	3.3/0.8	1.8/0.5
CESM_RCP8.5 (2086–2095)	22.9/16.6	3.9/1.2	2.1/0.6
CESM_CarbonCapture (2086–2095)	20.7/15.1	3.4/0.7	1.8/0.5
WACCM_RCP8.5 (2086–2095)	24.3/15.5	4.0/1.3	1.8/0.8
WACCM_SulfurInjection (2086–2095)	21.8/13.5	3.2/0.6	1.7/0.5

proximately scaled with the T increase will exacerbate future land aridity (Fu and Feng, 2014; Scheff and Frierson, 2014). Indeed, the projected P / PET under RCP8.5 (Fig. 3f) decreases over major land in both sets of model simulations, with a larger magnitude in CESM than WACCM (also seen in the last two columns of Table 2). The two geoengineering schemes can both limit PET growth (Fig. 3e) to reduce the tendency of worsening aridity but with considerably large differences in the magnitude and timing, as detailed below.

In terms of magnitude, carbon capture can lower the projected increase in PET by 60 % to 83 % at mid-century and the end of the century, respectively, which leads to an almost complete offset of P / PET decline (see green line in Fig. 3f). Therefore, the mid-century and end-of-century P / PET values are mostly the same as the present-day value, except for the near-term (prior to 2040) drop in P / PET due to the lagging effects of CO_2 mitigation, which will be elaborated later (Fig. 4). On the other hand, sulfur injection leads to a major decrease in PET that flips the sign of the projected increase due to GHG warming (Fig. 3e). For example, the mid-century projected PET increase is 102.2 mm yr^{-1}, but sulfur injection can reduce that by 127.8 mm yr^{-1}, which actually leads to a drop of the absolute value of PET by 25.6 mm yr^{-1}.

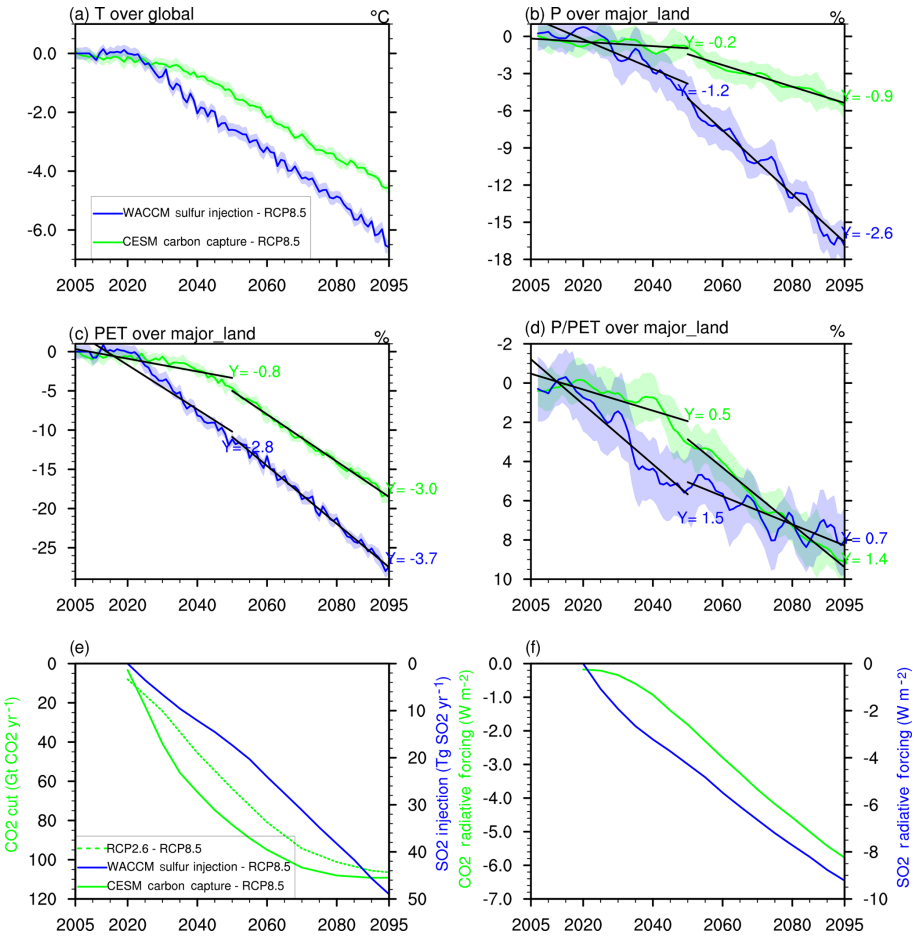

Figure 4. The changes in T, P, PET, and P / PET due to two types of geoengineering schemes. The changes are shown in relative terms (except for T in degrees Celsius), which are computed from the absolute values in Fig. 3. In panel **(d)**, the linear fit for the blue and green lines (separately for 2005–2050 and 2050–2095) is to highlight the near-term benefit of sulfur injection. **(e)** The mass of carbon cuts ($\mathrm{Gt\,CO_2\,yr^{-1}}$) and sulfur injection ($\mathrm{Tg\,SO_2\,yr^{-1}}$). The dashed green line is the RCP2.6 carbon cut for comparison; **(f)** the radiative forcing ($\mathrm{W\,m^{-2}}$) due to carbon capture and sulfate injection. The mass of carbon cuts and corresponding radiative forcing are based on Fig. 1 of Sanderson et al. (2017). The mass of sulfur injection comes from Fig. 2 of Tilmes et al. (2018). The sulfate radiative forcing is calculated based on the equations in Metzner et al. (2014).

The larger reduction in PET due to sulfur injection also is reflected in the larger increase in P / PET by 0.03 to 0.05, despite a smaller projected P / PET decline in the baseline WACCM warming.

The large response of P / PET due to sulfur injection to more than offset the baseline changes can be clearly seen in Fig. 3f (blue line). Different from all other curves, sulfur-injection-mitigated P / PET features an increase in absolute value, making the geoengineered climate over land overall "wetter" than the present day, despite a reduction in precipitation. Although both types of geoengineering can stabilize temperature at a level close to the present day, sulfur injection appears to have the additional benefit of flipping the sign of the drying trend as projected in the baseline scenarios.

Regarding timing, the increase in P / PET due to sulfur injection is mostly achieved in the near term (before 2050) due to the quick response time. Fig. 4b–d show the mitigation effects (the difference between the paired simulations) in percentage relative to the present day, which highlights the response due to two approaches in the near term and long term. During the first 30 years of the deployment (2020–2050), sulfur injection leads to a quicker reduction of PET of 2.8 % per decade than the decrease in P at 1.2 % per decade and thus causes the P / PET to increase (note the y axis for Fig. 4d is flipped to aid visual comparison). After 2050, when the precipitation decreases at a greater rate of 0.9 % per decade, the P / PET increase in response to sulfur injection will slow down (with the rate dropping by more than half from 1.5 to 0.7 % per decade). This nonmonotonic behavior in sulfur injection induced a P / PET response that is highly distinct from the carbon capture case in terms of timing. The latter, in contrast, always falls behind the sulfur injection changes

in inducing climate responses (green vs. blue in Fig. 4a–d). The P / PET enhancement due to carbon capture (compared to baseline warming, not to the present day) only starts to be significant toward the end of the century with a growth rate of 1.4 % per decade after 2050, almost 3 times larger than the decades before 2050.

3.4 Summary: faster and stronger benefits due to sulfur injection

In terms of mitigation at a global scale, we emphasize that P / PET is closely tied to land aridity conditions and vegetation response (Huang et al., 2017) rather than P itself. Note that we select P / PET among other drought indicators to avoid the complexity of the analysis because the main goal of our analysis is to compare highly extreme mitigation scenarios. Figure 2 reveals regional discrepancies suggesting that for a more comprehensive drought assessment, more metrics should be included in addition to P / PET.

Our results here suggest that sulfur injection not only offsets the projected worsening in aridity in the 21st century but also, surprisingly, leads to recovery from the present-day condition, which is already worse than preindustrial conditions or even just decades ago. More encouraging, the recovery ("wetting" over major global land) is detectable in the near term (MacMartin et al., 2019). Carbon capture, in contrast, has a weaker (even in relative terms) and slower mitigation benefit and does not lead to the full reversal of P / PET as in the response to sulfur injection. The response time of these two approaches is illustrated in Fig. 4e and f. Although the CO_2 reduction (Fig. 4e) has a quick increase after deployment (2020), radiative forcing due to the reduced CO_2 concentration (Fig. 4f) takes a slower trajectory to increase and is always falling behind the negative forcing due to sulfur injection.

The quicker and stronger response to sulfur injection suggests a benefit from deployment, providing a further incentive for adopting this scheme. However, because of the quicker response, one could counterargue that sulfur injection should be reserved as the "last resort" option only used when the CO_2 warming becomes too large towards the end of the century.

4 Regional responses in the Americas

How do the results and arguments above hold over specific regions? Next, we present a detailed comparison over North America and South America and discuss the mechanism. Other recent works have studied the precipitation response in various regions. Cheng et al. (2019), using soil moisture as the metric, have found major regions that would benefit from sulfur injection in having the aridity trend reversed. However, certain regions will have aridity conditions worsened in the sulfur injection scenario. Here we focus on North and South America using both P and P / PET to depict the full picture of hydrological response.

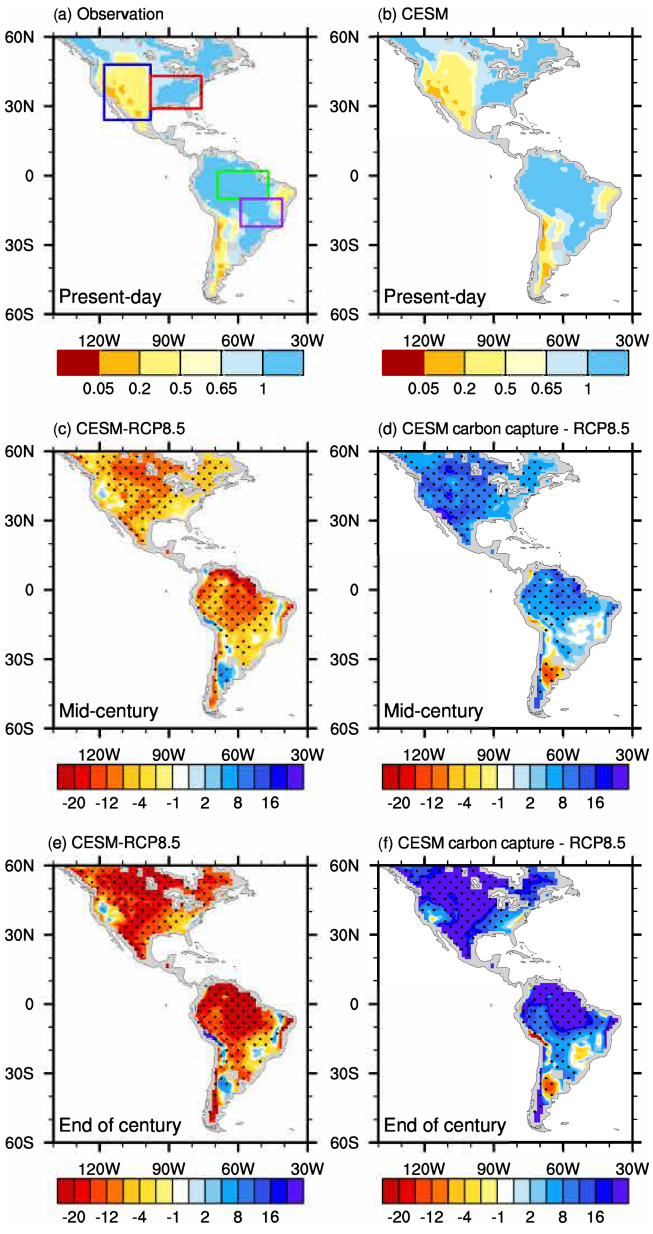

Figure 5. P / PET in the present day, the relative changes (%) in the future under RCP8.5, and mitigation due to carbon capture geoengineering using CESM. **(a, b)** The reanalysis and the bias-corrected output of the model in the present day (unitless). **(c)** The projected baseline changes relative to the present day (%); **(d)** the mitigation of the baseline changes relative to the present day. **(e, f)** Same as **(c, d)** but for the end of the century. The similar P / PET changes in absolute values (unitless) can be found in the top row of Fig. 2.

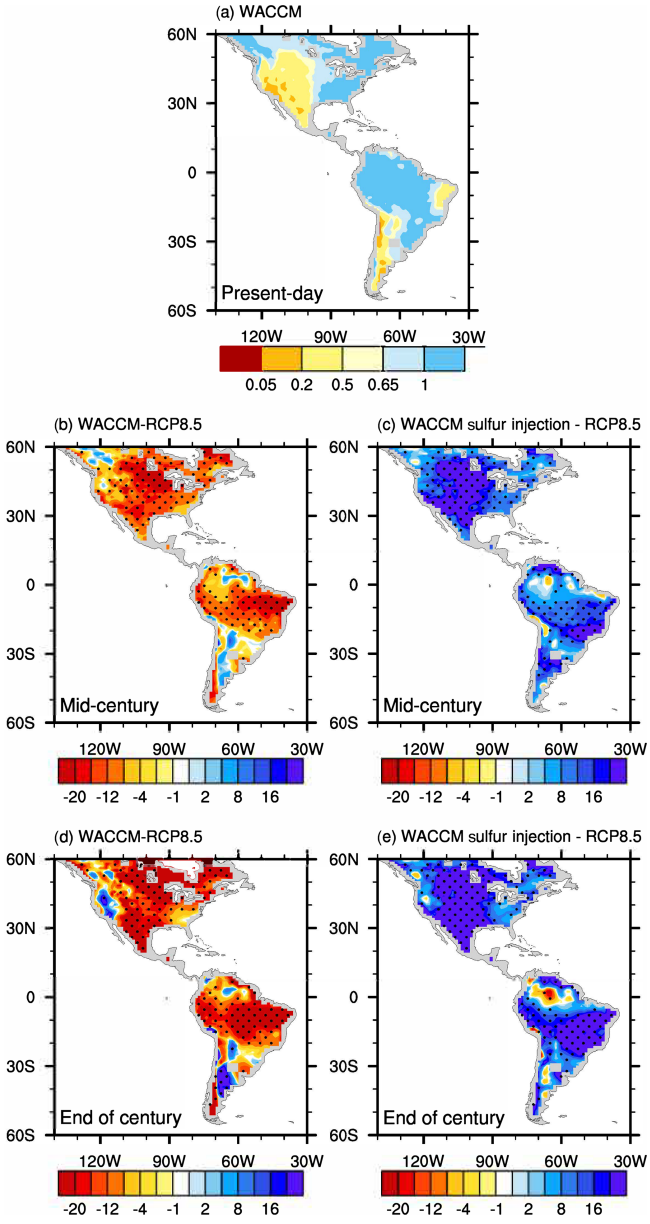

Figure 6. Same as Fig. 5, but for sulfur injection using WACCM. **(a)** P / PET in the bias-corrected output of the model in the present day (unitless). **(b)** The projected baseline changes at mid-century (%) relative to the present day; **(c)** the mitigation of the baseline changes relative to the present day. Panels **(d, e)** are the same as **(b, c)** but for the end of the century. The similar P / PET changes in absolute values (unitless) can be found in row 1 of Fig. 2.

4.1 North America

The main reason for focusing on North America is the arid land expansion from the American west into the Great Plains. The so-called 100th meridian, which traditionally separates the dry and mild climate, will likely shift eastward in future climate (Seager et al., 2018). This is clearly shown in the projection of both models, with a major decrease in P / PET over the Great Plains regions by 10 % to 20 % (Figs. 5 and 6). The corresponding change in absolute terms of P / PET is shown in Fig. 2. The slight increase (light blue) over the intermountain western US regions does not pass the significance test in being different from the baseline simulations.

For North America, it is clear that sulfur injection has a stronger effect than carbon capture, especially for the central US in the mid-century (Figs. 5 vs. 6). Towards the end of the century, sulfur injection increases P / PET by 0.05 (7.2 %), while carbon capture can eliminate the projected decrease in P / PET (Figs. 5 and 6). This is largely consistent with the results for the eastern US (although to a lesser extent for the latter) and the responses over global major land (Fig. 6, also illustrated in the time series in Fig. 3).

The large decrease in PET in response to sulfur injection is the main reason for a slight increase in P / PET compared to present-day conditions in the geoengineered cases. The P / PET changes over the US are consistent with the tendency of the global major land (Fig. 6d) and also largely supported by other metrics (soil water and P-ET in Fig. 6e, f).

Another way to examine the severity of aridity evolution is by further classifying the dryland into a few subtypes. These subtypes are classified by P / PET values, which are shown in the color bars in Fig. 5a and b. The global arid area (P / PET ranges of 0.2 to 0.5) would increase from 15 million km^2 in the historical period to 16.6 million km^2 under warming at the end of the century. Carbon capture can reduce it to 15.1 million km^2, but sulfur injection can more than offset it and lower it to 13.5 million km^2. Over North America, the results are generally similar, with a stronger reversal over the semiarid area (P / PET ranges of 0.5 to 0.65) due to sulfur injection than carbon capture.

4.2 South America

The main reason for focusing on South America is that drying over the Amazon (by more than 30 % using P / PET as the metric) could lead to die-out of the rainforest, decrease the carbon sink, and cause an increase in forest fires – major positive feedback that is missing in most of the global model projections so far, including the ones presented here.

While the changes over North America are largely consistent with global land change, South America's responses are more complicated. Notably, there is a major difference between northern Brazil, where the Amazon rainforest is mostly located, and the southern part of the nation (green and purple boxes in Fig. 5a).

Northern Brazil will see a major decline of P / PET of 0.2 to 0.4 (15 % to 30 % relative to the present day) in the baseline warming cases (Fig. 5), the largest among the four regions we considered in this study, transitioning the wetland into semiarid dryland. This large decline of P / PET is a result of both PET increase as in other regions and also a P decrease that is unique in this tropical land, in contrast to other regions examined. If the RCP8.5 projection turns out

to be true for the 21st century, a major consequence is the fate of the rainforest and its carbon uptake capacity. Given the high stakes, a relevant question is whether the two geoengineering schemes are able to reverse the drying trend over the Amazon.

The CESM results show that carbon capture can essentially overturn the baseline drying and keep the P / PET at the same level as the present day (Fig. 5). This is achieved by offsetting both the precipitation decrease and, more importantly, the projected PET increase by 80 % to 90 % (Fig. 7b, c). The carbon-capture-mitigated (green in Fig. 7b) climate will lead to a small increase in precipitation (relative to the present day) in northern Brazil, associated with a much smaller regional warming (<0.5 °C) than baseline (4.5 °C) (Fig. 5). Note that the regional precipitation change can be hard to project at the subcontinental scale, and thus the CESM-simulated carbon capture response could be model-dependent.

On the other hand, the WACCM results show that sulfur injection falls short of completely overturning the drying tendency over northern Brazil in the baseline warming but can mitigate the drying magnitude by 60 % by the end of the century. The reason for the insufficiency of sulfur injection is that, despite a substantial reduction in PET (Fig. 7c, from 0.8 to 0), the WACCM results continue to produce a stronger precipitation reduction (relative to the present day) in the case of sulfur injection (blue dots in Fig. 7b) but is unable to reverse the precipitation reduction in the warming baseline. This additional suppression of tropical rainfall due to sulfur injection is also previously reported in Simpson et al. (2019), who concluded that the dynamical response to stratospheric heating played an important role during JJA (but not in DJF).

Although the simultaneous reduction of PET in response to sulfur injection leads to the end result of wetting (in terms of P / PET increase; brown and blue points in Fig. 7d), the magnitude (roughly a 50 % offset) is small compared to that due to carbon capture (an offset by almost 100 %; green and red dots in Fig. 7d), for which the precipitation is flipped in sign to increase slightly rather than just with the baseline decrease mitigated (green in northern Brazil; Fig. 7b). Overall, there is a weaker mitigation of the P / PET drying trend in response to sulfur injection compared to carbon capture over northern Brazil. However, interestingly, the opposite is true for the sub-Amazon region, which is detailed below.

Unlike sulfur injection, carbon capture is consistently capable of mitigating the projected drying trend almost entirely over South America (similar to the global and eastern US cases). Despite being smaller than sulfur injection, there is sufficient capacity of carbon capture to overturn the drying trend over the sub-Amazon (from a 0.08 reduction of P / PET to almost zero), again due to a large reduction in PET despite slightly weakened precipitation. This suggests again that focusing on P alone may lead to a biased interpretation of the projected and mitigated trends. Notably, sulfur injection induces a much larger increase in P / PET (wetting) over the sub-Amazon compared to carbon capture, actually offsetting the projected P / PET decrease by 150 %. This is due to a regional increase in precipitation, which adds to PET reduction to cause a larger increase in P / PET. The mechanism is exactly the opposite of sulfur injection's smaller capacity (by only 60 %) to reverse the P / PET decline over the Amazon (northern Brazil), where the precipitation is projected to further decrease in response to sulfur injection despite a strong local cooling effect.

Synthesizing the precipitation changes over the Amazon (northern Brazil) and sub-Amazon (southern Brazil), the precipitation (especially in JJA as in Fig. 5 of Cheng et al., 2019) is shifted from the deep tropics to the subtropics in response to sulfur injection, leading to an actual increase in precipitation over the sub-Amazon by 36.5 mm yr^{-1} rather than just offsetting the 18.2 mm yr^{-1} decrease in the baseline warming case.

A substantial reduction in PET over the sub-Amazon (consistently true for other subregions explored in Fig. 7), working together with the precipitation increase, would induce a large increase in P / PET (0.2) relative to the baseline case, which is more than enough to offset the projected decrease of 0.15 and actually to lead to P / PET increase by 0.05. Considering that this region in the present day is already subject to a detectable drying, such an overcompensation in P / PET in response to sulfur injection should be viewed as beneficial to the regional climate and ecosystem, a point we have stressed for global mitigation results but want to echo again here for sub-Amazon regions.

4.3 Summary: unique responses over the Amazon (northern Brazil)

Overall, over three out of four regions examined here (western US, eastern US, and southern Brazil but not northern Brazil), sulfur injection has a larger capacity to not only mitigate but also flip the projected drying tendency. This is evidenced by the large response seen in the spatial maps in Fig. 6 (especially the larger response in the mid-century due to the time lag effects discussed in Sect. 3.1). A complete reversal to even an increase in P / PET drying highlights the benefit of sulfur injection, at least for these three regions. On the other hand, carbon capture can almost completely offset the P / PET change by 100 %, which is also the desired outcome. The mechanisms to achieve this complete offset can vary from one region to another and are sensitive to the regional precipitation projection in the baseline and mitigated scenarios (e.g., over the western US); they are thus potentially sensitive to model configurations. The responses over these three regions are found to be generally representative of the global mean (e.g., Fig. 7 major land, results with smaller error bars), which is presumably less subject to model diversity issues.

The South America regions illustrate a clear argument that a precipitation-centered viewpoint may mistakenly overesti-

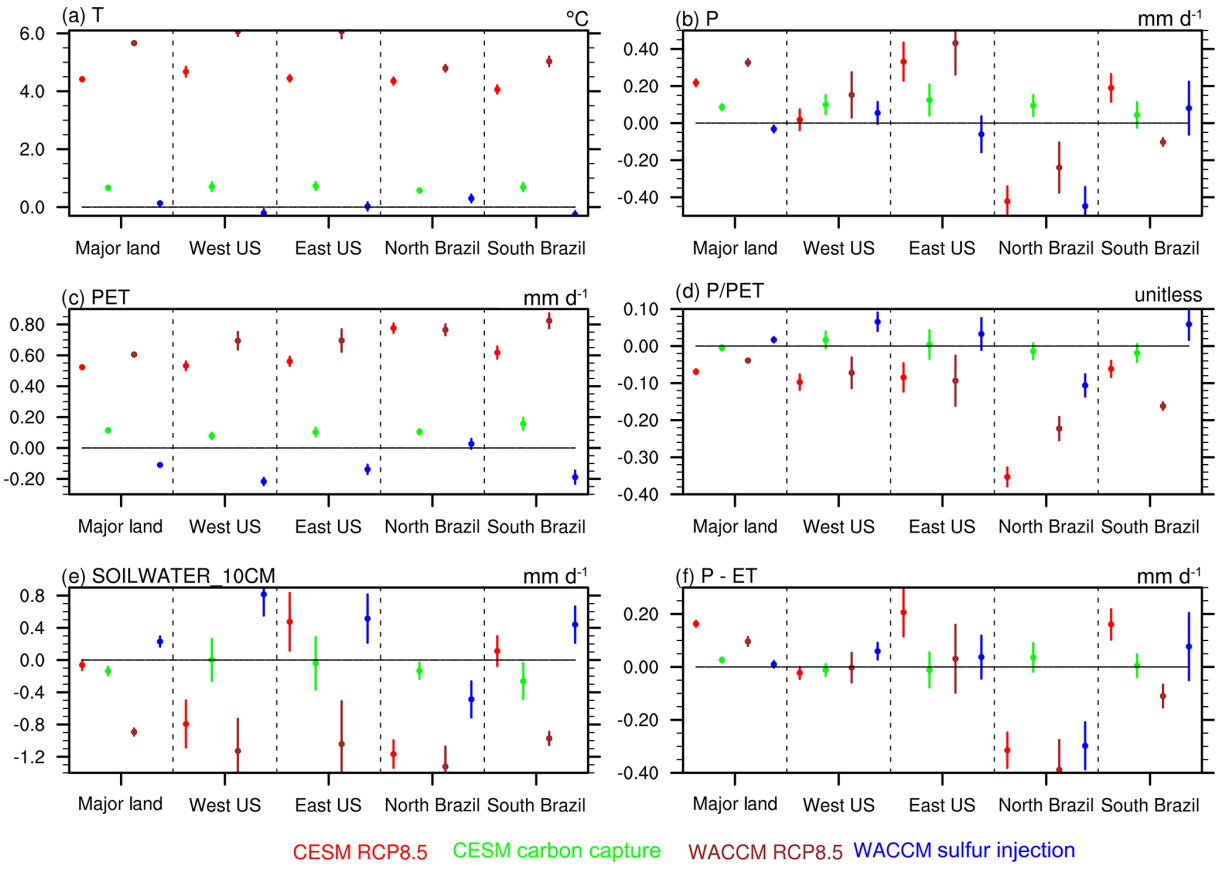

Figure 7. Regional changes at the end of the century relative to the present day. The western and eastern US are separated by 100° W, and northern and southern Brazil are separated by 10° S. See the boxes in Fig. 5a for the domains. The zero lines of the y axis indicate the present-day level.

mate sulfur injection side effects in causing aridity by ignoring the accompanying suppression of PET. The contrasting results for sulfur injection to overcome the global drying tendency, when using precipitation only or using P / PET, are clearly demonstrated for the Amazon region but are also similarly true for other regions such as the eastern US (to a lesser extent). For example, in Fig. 6, the precipitation change over the eastern US is slightly negative compared to the present day (overdrying) but becomes slightly positive in P / PET, suggesting an actual wetting, which is an improvement from the drying conditions already detectable in the present day (2010–2019) compared to the preindustrial era.

One exception to the summary above is northern Brazil (Amazon region). Sulfur injection, but not carbon capture, can only partially offset the projected drying due to a further decrease in precipitation locally in the deep tropics (Fig. 8b), which features a rainfall shift from the deep topics to subtropics (Fig. 6). In response to sulfur injection, there is a smaller amount of PET reduction from the baseline increase (Fig. 7c) compared to the other three regions and the global mean, presumably due to extensive cloud cover over the tropical land, but it could also be due to the vegetation difference between northern Brazil and southern Brazil.

5 Normalized changes with respect to global temperature change

The absolute value of climate benefits (including those presented in Table 2 and Fig. 7) is dependent on the strength of geoengineering measures and can thus be less useful in a broader context. What is more informative is the physical mechanism governing the changes. In order to elucidate the different mechanisms contributing to the simulated changes over North and South America, we next examine the individual climate variable contribution to P / PET changes in a normalized (% $°C^{-1}$) perspective.

In the following analysis, we show that even though sulfur injection has led to a larger mitigation benefit as detailed in the previous sections, it is mainly due to the larger forcing introduced and the larger global cooling realized (close to 6 °C). Sulfur injection is less effective in mitigating aridity worsening when the mitigation is normalized by the global cooling realized.

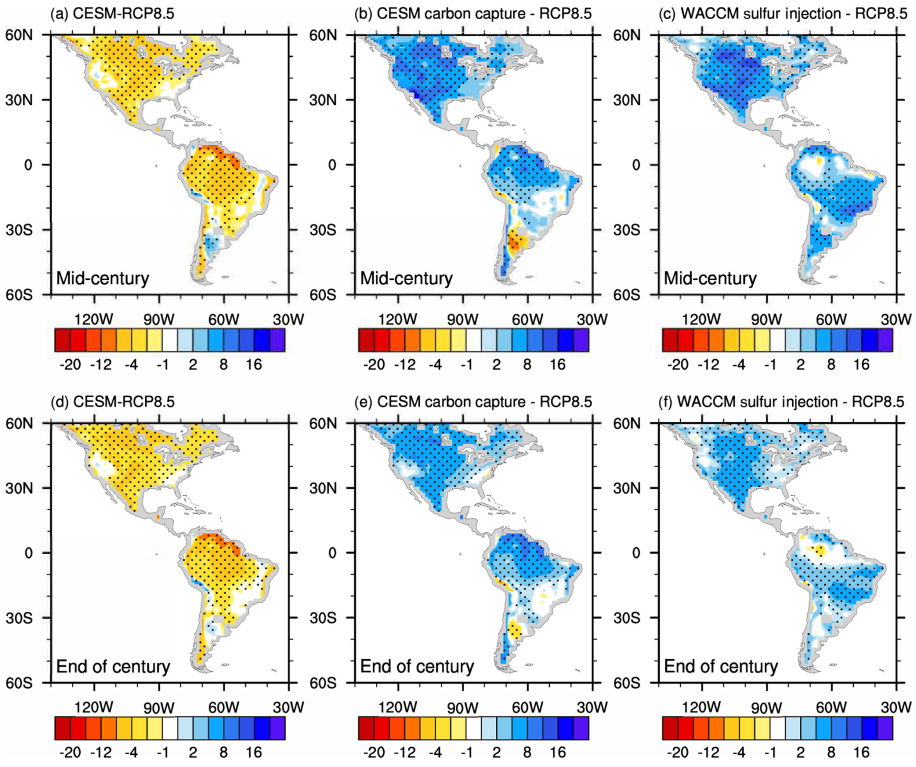

Figure 8. Similar to Fig. 5c–f but showing normalized P / PET change in percent per degree Celsius (% °C^{-1}). Panels **(a–c)** show mid-century changes, and panels **(d–f)** represent end-of-century changes. The normalization is by scaling the global temperature change in **(a, b, d, e)**, for example 4.2 °C due to carbon capture in panel **(e)** and 6.0 °C due to sulfur injection in panel **(f)**.

Figure 8 shows that the normalized changes have largely the same spatial pattern as in the absolute values presented in Fig. 5, but sulfur-injection-induced changes are now of a similar magnitude compared to the carbon capture case for both time periods, with a slightly larger value for the mid-century but smaller values at the end of the century. Note that because of the normalization, some of the Amazon and sub-Amazon regions have changes less than 1 % per degree Celsius (white area in Fig. 8) in response to carbon capture and sulfur injection, suggesting an insignificant change in aridity conditions if the global mean temperature mitigation is smaller than 1 °C. The Great Plains of the US, however, would benefit from either of the two geoengineering schemes, with a change as large as 5 to 10 % per degree Celsius.

What explains the weaker normalized P / PET response of sulfur injection? The relationship of various quantities (P, PET, P / PET) with respect to global mean temperature changes is further illustrated in the scatter plots (Fig. 9), with the slope representing the sensitivity of P, PET, and P / PET to global cooling induced by the two geoengineering schemes (4 to 6 °C of cooling on the x axis). The calculated slope using the linear fit in Fig. 9 is summarized in Table 4 and compared with another method of deriving the sensitivity using the epoch difference between the two end-of-century contrasting "epochs". Note that we have also tested the robustness of the linear regression approach by using the decadal mean (also shown in Table 4) or annual mean (as in Fig. 9), which turns out to yield a small difference. For example, the precipitation sensitivity changes from 2.6 % per degree Celsius (Fig. 9a) to 2.7 % per degree Celsius at a global scale (Table 4).

The larger sensitivity in precipitation due to sulfur injection (Fig. 9) is well-understood (Muri et al., 2018; Niemeier et al., 2013; Kleidon et al., 2015) as a distinct feature of fast adjustment to stratospheric aerosol forcing (and also solar forcing as indicated in many previous studies, such as Bala et al., 2009; Duan et al., 2018). The large sensitivity to aerosols is also largely consistent with previous results contrasting tropospheric SO_2 and CO_2 increase (e.g., Ming and Ramaswamy, 2007; Wang et al., 2017b). The larger slope of precipitation due to sulfur injection in WACCM is consistent with our previous study (Lin et al., 2016), but the magnitude of the response is smaller than that reported in a different model (CESM1) forced by the 20th-century tropospheric aerosol changes (Table 4; 6.7 % per degree Celsius). In contrast, carbon-capture-induced precipitation response (1.1 % per degree Celsius) is of similar magnitude when compared with the 20th-century CO_2 increase examined with the same model (CESM1 in Lin et al., 2016; 1.2 % per degree Celsius).

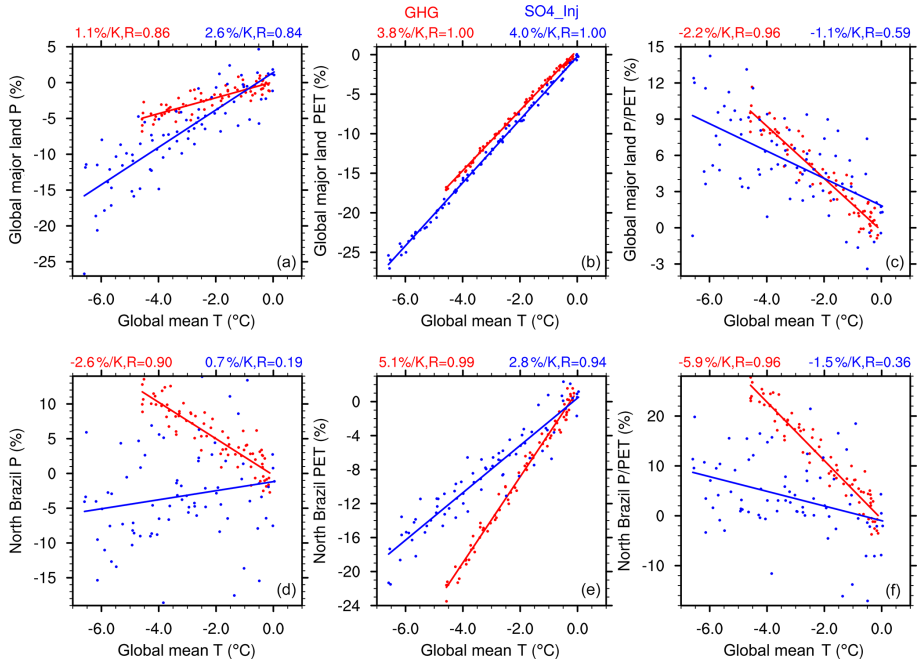

Figure 9. The changes in global major land P, PET, and P / PET as a function of global mean temperature change (ocean + land). Each dot represents a model year during 2020–2097. Red is for carbon capture (using CESM), and blue is for sulfur injection (using WACCM). **(a, b, c)** Global land; **(d, e, f)** northern Brazil.

Different from the precipitation sensitivity, the PET sensitivities to carbon capture and sulfur injection are similar (3.8 vs. 4 % per degree Celsius). A similar PET change, when combined with the greater precipitation decrease, will lead to a smaller increase in P / PET in response to sulfur injection. In other words, the almost identical PET sensitivity in response to sulfur injection and carbon capture is the main reason that sulfur injection has a smaller control over P / PET by a factor of 2 (Fig. 9; −1.1 vs. −2.2 % per degree Celsius). If sulfur injection leads to a greater amount of surface radiation reduction in other models such as CESM1 as in Lin et al. (2016), the P / PET sensitivity due to sulfur injection could be as large as the carbon capture case here. For example, Lin et al. (2016) previously found that tropospheric SO_2 will lead to a much stronger PET sensitivity (6.3 % per degree Celsius) than CO_2 (4.6 % per degree Celsius) because of the surface solar radiation reduction. In this study, the PET response to sulfur injection (4 % per degree Celsius) is only slightly higher than that due to carbon capture (3.5–3.8 % per degree Celsius depending on the method of normalization).

Another complexity arises. Our previous 20th-century-based analysis (Lin et al., 2016) shows that tropospheric sulfate-induced PET changes strongly by 6.3 % per degree Celsius. However, it still falls short of compensating for the large precipitation decrease by 6.7 % per degree Celsius, thus producing a small decline of P / PET (by only 0.4 % per degree Celsius) in response to tropospheric sulfate cooling, opposite to the larger increase in P / PET in response to stratospheric sulfur injection (−1.5 % per degree Celsius). The current model experiment precludes a solution to the discrepancy of sulfur-induced P, PET, and P / PET responses because of model difference (WACCM here vs. CESM in Lin et al., 2016) and forcing difference (stratospheric here vs. tropospheric in Lin et al., 2016). We speculate that the difference is mainly from the forcing difference because stratospheric aerosols can be less effective in changing surface energy balance than tropospheric aerosols, which can induce warm cloud changes and are more concentrated over the land.

The speculation above is worth testing, for example using the volcanic forcing experiment in the Last Millennium Ensemble (LME, using CESM but with 2° resolution; Fu et al., 2017). Our analysis in Table 4 supports this argument. The GHG-only and aerosol-only results from LME are similar to the Lin et al. (2016) results of CO_2- and SO4-induced responses using the same model (but with 1° resolution). Volcanic eruptions (active during the three periods of 1250–1270, 1450–1460, and 1800–1820) before 1850 induced a much weaker P response (2.5 to 4 % per degree Celsius) than tropospheric SO_2, similar to the sulfur injection results reported here (but using the different model of WACCM). Also, what is similar to the sulfur injection results here, despite the model difference, is the overall increase in P / PET when stratospheric aerosol cooling is imposed (i.e., negative sensitivity of P / PET in Table 4), suggesting that the "benefit" of flipping the projected P / PET decrease via stratospheric sulfur injection could be robust and model-independent.

Table 4. Global major land changes in P, PET, and P / PET normalized by global temperature change. Two methods are used here: the first method is comparing the epoch difference of the end-of-century climate to obtain the normalized response. The second method is conducting a linear regression over the decadal time series of anomaly induced by carbon capture or sulfur injection. In the rightmost columns, we contrast the results with the response to atmospheric CO_2, tropospheric SO_4 in the 20th century, and the various forcing experiments in the Last Millennium Ensemble (LME). The value after ± is 1 standard deviation; n/a: not applicable.

P (% °C^{-1})	Carbon capture	Sulfur injection	CO_2 (Lin et al., 2016)	Trop. SO_2 (Lin et al., 2016)	LME GHG	LME O3 and AER	LME volcanic 1250–1270, 1450–1460, 1800–1820
Epoch difference	1.1 ± 1.9	2.4 ± 2.2	1.2 ± 0.4	6.7 ± 1.5	1.4 ± 2.3	8.1 ± 2.9	2.6 ± 12.0/4.1 ± 7.9/ 2.5 ± 10.0
Linear regression	1.1 ± 0.9	2.7 ± 3.3	n/a	n/a	n/a	n/a	n/a
PET (% °C^{-1})							
Epoch difference	3.5 ± 2.9	4.0 ± 2.1	4.6 ± 0.2	6.3 ± 0.4	4.2 ± 0.8	7.7 ± 1.4	7.2 ± 10.8/6.4 ± 6.8/ 5.6 ± 6.9
Linear regression	3.8 ± 0.3	4.0 ± 0.4	n/a	n/a	n/a	n/a	n/a
P / PET (% °C^{-1})							
Epoch difference	−2.0 ± 2.0	−1.5 ± 1.7	−3.3 ± 0.5	0.4 ± 1.6	−2.7 ± 2.6	0.3 ± 4.1	−4.9 ± 10.4/−2.5 ± 7.2/ −3.2 ± 9.3
Linear regression	−2.2 ± 1.0	−1.1 ± 3.1	n/a	n/a	n/a	n/a	n/a

Table 5. Change (% °C^{-1}) in PET and P / PET due to contributions of other climate variables (RH2M, $U10$, T, Rn-G, P). The variables used for this table are not bias-corrected because of the lack of a reliable benchmark for $U10$ and Rn-G (surface-available energy, which is the incoming radiation reaching the ground minus the heat flux into the ground).

(a) Contribution to PET change

Carbon capture/ sulfur injection (% °C^{-1})	RH2M (relative humidity at 2 m)	$U10$ (surface wind at 10 m)	T	Rn-G (surface available energy)
Global major land	0.7/0.4	0.1/0.2	3.2/3.0	1.0/1.4
Northern Brazil	1.4/0.4	0.3/0.0	2.3/1.6	2.2/1.6
Southern Brazil	0.8/1.2	0.0/0.6	2.3/2.3	1.1/0.8

(b) Contribution to P / PET change

Carbon capture/ sulfur injection (% °C^{-1})	RH2M (relative humidity)	$U10$ (surface wind)	T	Rn-G (surface available energy)	P
Global major land	−0.7/−0.4	−0.1/−0.2	−2.7/−2.6	−0.8/−1.3	1.7/3.0
Northern Brazil	−1.1/−0.3	−0.2/0.0	−1.5/−1.2	−1.6/−1.3	−3.4/0.9
Southern Brazil	−0.7/−1.1	0.0/−0.4	−1.9/−1.8	−1.0/−0.7	1.6/−1.0

In Table 5, we further break down the induced PET and P / PET changes (% °C^{-1}) into four key quantities that contribute to PET calculation. The surface wind and relative humidity are, in general, smaller contributors compared with T and surface energy, except that at the regional level RH can increase in response to cooling and thus reduce the PET. The stronger surface energy perturbation due to sulfur injection compared to carbon capture, mainly due to the strong suppression of incoming solar radiation reaching the ground, is clearly a major contributor to the larger reduction of PET at a global level, but not so for South America (Fig. 10), presumably due to the extensive background cloud covers. Similarly, the changes in P over South America are complicated (Fig. 10), featuring a decrease in northern Brazil rainfall given the sulfur injection cooling (0.9 % per degree Celsius) but an increase in response to the carbon capture cooling.

To summarize, the weaker sensitivity of P / PET in response to sulfur injection globally and the weaker response in absolute values over the Amazon region, as shown in Sect. 4, are the two major counterarguments against the effectiveness of sulfur injection. The comparison with our earlier studies on tropospheric SO_2 and volcanic eruptions using different model configurations (the 20th century or last millennium; CESM with 1° or 2° resolution) demonstrates the qualitative robustness of the results and the common physical mechanisms.

6 Concluding remarks

By examining the response of land hydroclimate to two types of geoengineering approaches, we show that sulfur injection will lead to land wetting when the metric in use is P / PET instead of P. An additional promising feature is that sulfur injection can lead to a more rapid response in the next few decades, while the benefit is only gradually getting stronger in the case of carbon capture despite an earlier effort to lower emissions. Even though the mitigation from the two approaches is introduced around 2020 in these two experiments, the short-term (next 30 years) effect is stronger in the case of sulfur injection migration. The response time difference is due to the short-lived nature of sulfate aerosols, which will respond to mitigation measures more rapidly than long-lived species of CO_2. However, we also point out the weaker efficiency of reversing Amazon drying due to the further precipitation shift away from the deep tropics to extratropics in response to sulfur injection. Moreover, we show that on a per-degree-cooling basis, sulfur injection is less effective than carbon capture at offsetting the drying tendency globally and more so regionally over the Amazon (Fig. 9d–f), again because of the stronger precipitation suppression.

An important note should be made regarding the interpretation of the quantitative benefits presented. Because these two models have different climate sensitivities, the baseline warming induced by unchecked emissions growth is not at the same level. WACCM warms faster, reaches the 2 °C level in earlier decades, and has higher end-of-century warming at 6 °C compared to CESM. Since the baseline warming is different for the two models in different decades, the climate benefit due to any mitigation measures should also be interpreted in a relative sense, i.e., the fraction (%) of the projected change in the future that can be mitigated by carbon capture or sulfur injection. For example, even if our results suggest that sulfur injection can lead to a 5–6 °C cooling, while carbon capture can lead to a 4–5 °C cooling, that does not quantitatively provide any constraints on the strength of the respective approaches.

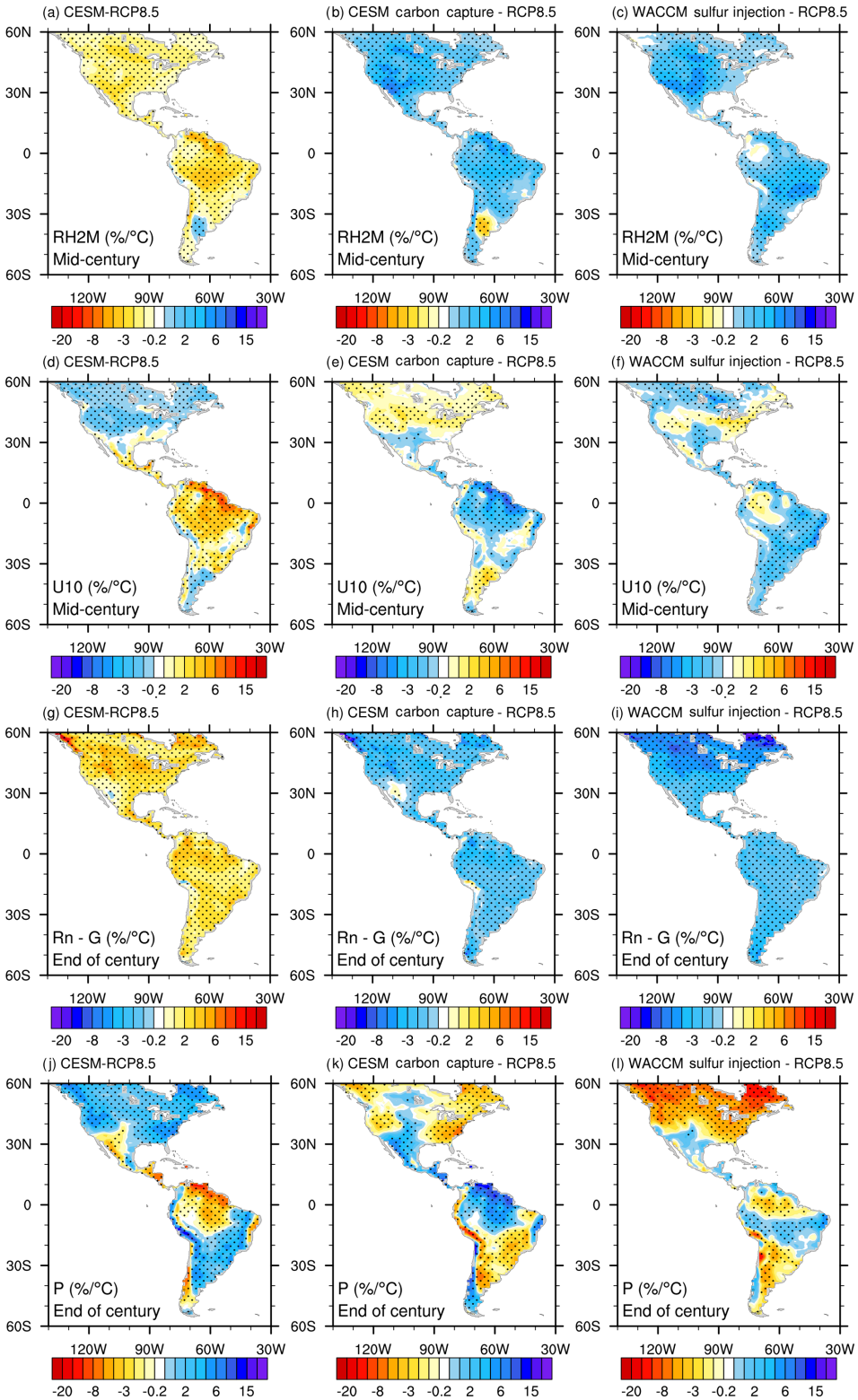

Figure 10. Similar to Fig. 8 but showing RH2M (row 1; relative humidity, normalized change in percent per degree Celsius), $U10$ (row 2; surface wind, normalized change in percent per degree Celsius), Rn-G (row 3; surface-available energy, normalized change in percent per degree Celsius), and P (row 4; precipitation, normalized change in percent per degree Celsius). Left panels show the changes in baseline warming. Middle panels show mitigated change due to carbon capture. Right panels show the mitigated change due to sulfur injection. Note that, for simplicity, we only show RH2M and $U10$ results for the mid-century, as well as Rn-G and P results for the end of the century.

We further note that the strength of each geoengineering approach, even when expressed in relative terms, is subject to the assumption of applied forcing and/or perturbation. For example, the climate benefit can be enhanced by applying a larger sulfur injection or deploying carbon capture in a greater amount or earlier. In fact, in an earlier project that conducted similar carbon capture experiments (Sanderson et al., 2017), a weaker version of decarbonization was presented (by applying a smaller amount of emission cuts and carbon capture), under which the temperature temporarily exceed the 2 °C level during the 21st century (i.e., "overshoot") before falling back to a stabilized 1.5 °C level.

As a result, we emphasize that the main purpose of this paper is not to examine the effectiveness of these two climate engineering schemes in terms of absolute values. Instead, we aim to highlight the physical mechanisms at play, especially when they are distinct between the two approaches (e.g., radiative balances and dynamic response). The notable distinctions between the two approaches include response timescales, the role of solar dimming at the surface, and the shift of deep tropical rainfall. The direct physiological role of CO_2 is potentially important because the CO_2 level is not reduced in the sulfur injection approach. But this study, focusing on meteorological drivers of land aridity using P / PET, did not delve into the physiological effect of CO_2 on plant transpiration via stomatal closure, which also appears to be weak in these two models compared with other climate models (Swann et al., 2018).

The analytical framework established here will thus (1) help to understand the contrasting response in terms of spatial and temporal distribution, which goes beyond the specific regions highlighted here, and (2) provide broader insights into the mitigation impact of other geoengineering approaches beyond the two discussed here (such as cirrus ice cloud thinning or marine warm cloud brightening, Muri et al., 2018; and surface albedo modifications, Crook et al., 2015; space mirror, Niemeier et al., 2013).

The quantitative results here using a suite of climate models thus need to be interpreted through the lens of model diversity. A recent example of such an attempt using two global climate models (Laakso et al., 2020) focused on the global mean precipitation response to carbon extraction and sulfur injection. Some aspects of the simulated responses here (e.g., the weaker sensitivity of precipitation to sulfur injection in WACCM) are worth revisiting by conducting systematic experiments using other climate models, such as the newly available CESM2 (WACCM6). To place the two types of geoengineering schemes in a broader context, future research is also needed to further examine the upcoming model output from GeoMIP6 (the Geoengineering Model Intercomparison Project Phase 6) and CDRMIP.

Data availability. All GLENS data are available to the community via the Earth System Grid (http://www.cesm.ucar.edu/projects/community-projects/GLENS/, GLENS, 2020).

The 1.5 and 2 °C target simulation data are available at http://www.cesm.ucar.edu/experiments/1.5-2.0-targets.html (CESM, 2020).

Author contributions. YX designed and coordinated the research. LL conducted the data analysis with partial assistance from CD. YX wrote the paper with input from all co-authors.

Competing interests. The authors declare that they have no conflict of interest.

Acknowledgements. The CESM project is supported primarily by the National Science Foundation (NSF). Computing and data storage resources, including the Cheyenne supercomputer (https://doi.org/10.5065/D6RX99HX), were provided by the Computational and Information Systems Laboratory (CISL) at NCAR.

Review statement. This paper was edited by Govindasamy Bala and reviewed by three anonymous referees.

Financial support. Lei Lin is supported by the National Key Research and Development Program of China (grant no. 2016YFA0602701). Yangyang Xu and Chenrui Diao are supported by NSF grant no. 1841308. The modeling run was done by the National Center for Atmospheric Research (NCAR), which is a major facility sponsored by the NSF under cooperative agreement no. 1852977.

References

Bala, G., Duffy, P. B., and Taylor, K. E.: Impact of geoengineering schemes on the global hydrological cycle, P. Natl. Acad. Sci. USA, 105, 7664–7669, 2008.

Bala, G., Caldeira, K., and Nemani, R.: Fast versus slow response in climate change: implications for the global hydrological cycle, Clim. Dynam., 35, 423–434, https://doi.org/10.1007/s00382-009-0583-y, 2010.

Cao, L., Duan, L., Bala, G., and Caldeira, K.: Simultaneous stabilization of global temperature and precipitation through cocktail geoengineering, Geophys. Res. Lett., 44, 7429–7437, https://doi.org/10.1002/2017GL074281, 2017.

Chen, M., Xie, P., Janowiak, J. E., and Arkin, P. A.: Global Land Precipitation: A 50-yr Monthly Analysis Based on Gauge Observations, J. Hydrometeorol., 3, 249–266, https://doi.org/10.1175/1525-7541(2002)003<0249:GLPAYM>2.0.CO;2, 2002.

Cheng, W., MacMartin, D. G., Dagon, K., Kravitz, B., Tilmes, S., Richter, J. H., Mills, M. J., and Simpson, I. R.: Soil Moisture and Other Hydrological Changes in a Stratospheric Aerosol Geoengi-

neering Large Ensemble, J. Geophys. Res.-Atmos., 124, 12773–12793, https://doi.org/10.1029/2018JD030237, 2019.

CESM: CESM Simulations to study climate under 1.5 °C and 2.0 °C targets: available at: http://www.cesm.ucar.edu/experiments/1.5-2.0-targets.html, last access: 29 July 2020.

Crook, J. A., Jackson, L. S., Osprey, S. M., and Forster, P. M.: A comparison of temperature and precipitation responses to different Earth radiation management geoengineering schemes, J. Geophys. Res.-Atmos., 120, 9352–9373, https://doi.org/10.1002/2015JD023269, 2015.

Crutzen, P. J.: Albedo Enhancement by Stratospheric Sulfur Injections: A Contribution to Resolve a Policy Dilemma?, Climate Change, 77, 211–220, https://doi.org/10.1007/s10584-006-9101-y, 2006.

Dai, A.: Characteristics and trends in various forms of the Palmer Drought Severity Index during 1900–2008, J. Geophys. Res., 116, D12115, https://doi.org/10.1029/2010JD015541, 2011.

Duan, L. C., Bala, G., and Caldeira, K.: Comparison of the Fast and Slow Climate Response to Three Radiation Management Geoengineering Schemes, J. Geophys. Res.-Atmos., 10.1029/2018JD029034, 2018.

Donat, M. G., Alexander, L. V, Yang, H., Durre, I., Vose, R., Dunn, R. J. H., Willett, K. M., Aguilar, E., Brunet, M., Caesar, J., Hewitson, B., Jack, C., Klein Tank, A. M. G., Kruger, A. C., Marengo, J., Peterson, T. C., Renom, M., Oria Rojas, C., Rusticucci, M., Salinger, J., Elrayah, A. S., Sekele, S. S., Srivastava, A. K., Trewin, B., Villarroel, C., Vincent, L. A., Zhai, P., Zhang, X., and Kitching, S.: Updated analyses of temperature and precipitation extreme indices since the beginning of the twentieth century: The HadEX2 dataset, J. Geophys. Res.-Atmos., 118, 2098–2118, https://doi.org/10.1002/jgrd.50150, 2013.

Easterling, D. R.: Climate Extremes: Observations, Modeling, and Impacts, Science, 289, 2068–2074, https://doi.org/10.1126/science.289.5487.2068, 2000.

Effiong, U. and Neitzel, R. L.: Assessing the direct occupational and public health impacts of solar radiation management with stratospheric aerosols, Environ. Heal., 15, 7, https://doi.org/10.1186/s12940-016-0089-0, 2016.

Fan, Y. and van den Dool, H.: A global monthly land surface air temperature analysis for 1948–present, J. Geophys. Res., 113, D01103, https://doi.org/10.1029/2007JD008470, 2008.

Feng, S. and Fu, Q.: Expansion of global drylands under a warming climate, Atmos. Chem. Phys., 13, 10081–10094, https://doi.org/10.5194/acp-13-10081-2013, 2013.

Field, L., Ivanova, D., Bhattacharyya, S., Mlaker, V., Sholtz, A., Decca, R., Manzara, A., Johnson, D., Christodoulou, E., Walter, P., and Katuri, K.: Increasing Arctic sea ice albedo using localized reversible geoengineering, Earth's Future, 6, 882–901, https://doi.org/10.1029/2018EF000820, 2018.

Fischer, E. M. and Knutti, R.: Anthropogenic contribution to global occurrence of heavy-precipitation and high-temperature extremes, Nat. Clim. Chang., 5, 560–564, https://doi.org/10.1038/nclimate2617, 2015.

Fu, Q. and Feng, S.: Responses of terrestrial aridity to global warming, J. Geophys. Res.-Atmos., 119, 7863–7875, https://doi.org/10.1002/2014JD021608, 2014.

Fu, Q., Lin, L., Huang, J., Feng, S., and Gettelman, A.: Changes in terrestrial aridity for the period 850-2080 from the Community Earth System Model, J. Geophys. Res.-Atmos., 121, https://doi.org/10.1002/2015JD024075, 2016.

Gettelman, A., Mills, M. J., Kinnison, D. E., Garcia, R. R., Smith, A. K., Marsh, D. R., Tilmes, S., Vitt, V., Bardeen, C. G. , McInerny, J., Liu, H.-L., Solomon, S. C., Polvani, L. M., Emmons, L. K., Lamarque, J.-F., Richter, J. H., Glanville, A. S., Bacmeister, J. T., Phillips, A. S., Neale, R. B., Simpson, I. R., DuVivier, A. K., Hodzic, A., and Randel, W. J.: The whole atmosphere community climate model version 6 (WACCM6), J. Geophys. Res.-Atmos., 124, 12380–12403, https://doi.org/10.1029/2019JD030943, 2019.

Hanna, R., Xu, Y., and Victor, D. G.: After COVID-19, green investment must deliver jobs to get political traction, Nature, 582, 178–180, https://doi.org/10.1038/d41586-020-01682-1, 2020.

Helwegen, K. G., Wieners, C. E., Frank, J. E., and Dijkstra, H. A.: Complementing CO_2 emission reduction by solar radiation management might strongly enhance future welfare, Earth Syst. Dynam., 10, 453–472, https://doi.org/10.5194/esd-10-453-2019, 2019.

Herzog, H. J.: Peer Reviewed: What Future for Carbon Capture and Sequestration?, Environ. Sci. Technol., 35, 148A–153A, https://doi.org/10.1021/es012307j, 2001.

Hu, A., Xu, Y., Tebaldi, C., Washington, W. M., and Ramanathan, V.: Mitigation of short-lived climate pollutants slows sea-level rise, Nat. Clim. Chang., 3, 730–734, https://doi.org/10.1038/nclimate1869, 2013.

Huang, J., Li, Y., Fu, C., Chen, F., Fu, Q., Dai, A., Shinoda, M., Ma, Z., Guo, W., Li, Z., Zhang, L., Liu, Y., Yu, H., He, Y., Xie, Y., Guan, X., Ji, M., Lin, L., Wang, S., Yan, H., and Wang, G.: Dryland climate change: Recent progress and challenges, Rev. Geophys., 55, 719–778, https://doi.org/10.1002/2016RG000550, 2017.

Hulme, M.: Recent Climatic Change in the World's Drylands, Geophys. Res. Lett. 23, 61–64, https://doi.org/doi:10.1029/95GL03586, 1996.

Irvine, P. J., Kravitz, B., Lawrence, M. G., Gerten, D., Caminade, C., Gosling, S. N., Hendy, E. J., Kassie, B. T., Kissling, W. D., Muri, H., Oschlies, A., and Smith, S. J.: Towards a comprehensive climate impacts assessment of solar geoengineering, Earth's Future, 5, 93–106, https://doi.org/10.1002/2016EF000389, 2017.

Jones, A., Haywood, J. M., Alterskjær, K., Boucher, O., Cole, J. N. S., Curry, C. L., Irvine, P. J., Ji, D., Kravitz, B., Kristjánsson, J. E., Moore J. C., Niemeier, U., Robock, A., Schmidt, H., Singh, B., Tilmes, S., Watanabe, S., and Yoon, J. H.: The impact of abrupt suspension of solar radiation management (termination effect) in experiment G2 of the Geoengineering Model Intercomparison Project (GeoMIP), J. Geophys. Res.- Atmos., 118, 9743–9752, doi:10.1002/jgrd.50762, 2013.

Kay, J. E., Deser, C., Phillips, A., Mai, A., Hannay, C., Strand, G., Arblaster, J. M., Bates, S. C., Danabasoglu, G., Edwards, J., Holland, M., Kushner, P., Lamarque, J.-F., Lawrence, D., Lindsay, K., Middleton, A., Munoz, E., Neale, R., Oleson, K., Polvani, L., and Vertenstein, M.: The Community Earth System Model (CESM) Large Ensemble Project: A Community Resource for Studying Climate Change in the Presence of Internal Climate Variability. B. Am. Meteorol. Soc., 96, 1333–1349. https://doi.org/10.1175/BAMS-D-13-00255.1, 2015.

Keller, D. P., Feng, E. Y., and Oschlies, A.: Potential climate engineering effectiveness and side effects during a high

carbon dioxide-emission scenario, Nat. Commun., 5, 3304, https://doi.org/10.1038/ncomms4304, 2014.

Kleidon, A., Kravitz, B., and Renner, M.: The hydrological sensitivity to global warming and solar geoengineering derived from thermodynamic constraints, Geophys. Res. Lett., 42, 138–144, https://doi.org/10.1002/2014GL062589, 2015.

Knapp, A. K., Beier, C., Briske, D. D., Classen, A. T., Luo, Y., Reichstein, M., Smith, M. D., Smith, S. D., Bell, J. E., Fay, P. A., Heisler, J. L., Leavitt, S. W., Sherry, R., Smith, B., and Weng, E.: Consequences of More Extreme Precipitation Regimes for Terrestrial Ecosystems, Bioscience, 58, 811–821, https://doi.org/10.1641/B580908, 2008.

Kravitz, B., MacMartin, D. G., Mills, M. J., Richter, J. H., Tilmes, S., Lamarque, J.-F., Tribbia, J. J., and Vitt, F.: First Simulations of Designing Stratospheric Sulfate Aerosol Geoengineering to Meet Multiple Simultaneous Climate Objectives, J. Geophys. Res.-Atmos., 122, 12616–12634, https://doi.org/10.1002/2017JD026874, 2017.

Kravitz, B., Robock, A., and Irvine, P.: Robust Results From Climate Model Simulations of Geoengineering, EOS T. Am. Geophys. Un., 94, 292–292, https://doi.org/10.1002/2013EO330005, 2013.

Kunkel, K. E., Pielke, R. A., and Changnon, S. A.: Temporal Fluctuations in Weather and Climate Extremes That Cause Economic and Human Health Impacts: A Review, B. Am. Meteorol. Soc., 80, 1077–1098, https://doi.org/10.1175/1520-0477(1999)080<1077:TFIWAC>2.0.CO;2, 1999.

Laakso, A., Snyder, P. K., Liess, S., Partanen, A.-I., and Millet, D. B.: Differing precipitation response between solar radiation management and carbon dioxide removal due to fast and slow components, Earth Syst. Dynam., 11, 415–434, https://doi.org/10.5194/esd-11-415-2020, 2020.

Lawrence, M. G., Schäfer, S., Muri, H., Scott, V., Oschlies, A., Vaughan, N. E., Boucher, O., Schmidt, H., Haywood, J., and Scheffran, J.: Evaluating climate geoengineering proposals in the context of the Paris Agreement temperature goals, Nat. Commun., 9, 3734, https://doi.org/10.1038/s41467-018-05938-3, 2018.

Lesk, C., Rowhani, P., and Ramankutty, N.: Influence of extreme weather disasters on global crop production, Nature, 529, 84–87, https://doi.org/10.1038/nature16467, 2016.

Lin, S.-J.: A "Vertically Lagrangian" Finite-Volume Dynamical Core for Global Models, Mon. Weather Rev., 132, 2293–2307, https://doi.org/10.1175/1520-0493(2004)132<2293:AVLFDC>2.0.CO;2, 2004.

Lin, L., Gettelman, A., Xu, Y., and Fu, Q.: Simulated responses of terrestrial aridity to black carbon and sulfate aerosols, J. Geophys. Res. -Atmos., 121(2), 785–794, doi:10.1002/2015JD024100, 2016.

Lin, L., Wang, Z., Xu, Y., Zhang, X., Zhang, H., and Dong, W.: Additional Intensification of Seasonal Heat and Flooding Extreme Over China in a 2 °C Warmer World Compared to 1.5 °C, Earth's Future, 6, 968–978, https://doi.org/10.1029/2018EF000862, 2018.

MacMartin, D. G., Kravitz, B., Tilmes, S., Richter, J. H., Mills, M. J., Lamarque, J.-F., Tribbia, J. J., and Vitt, F.: The Climate Response to Stratospheric Aerosol Geoengineering Can Be Tailored Using Multiple Injection Locations, J. Geophys. Res.-Atmos., 122, 12574–12590, https://doi.org/10.1002/2017JD026868, 2017.

MacMartin, D. G., Ricke, K. L., and Keith, D. W.: Solar geoengineering as part of an overall strategy for meeting the 1.5 °C Paris target, Philos. T. Roy. Soc. A., 376, 20160454, https://doi.org/10.1098/rsta.2016.0454, 2018.

MacMartin, D. G., Wang, W., Kravitz, B., Tilmes, S., Richter, J. H., and Mills, M. J.: Timescale for detecting the climate response to stratospheric aerosol geoengineering, J. Geophys. Res.-Atmos., 124, 1233–1247, https://doi.org/10.1029/2018JD028906, 2019.

Meinshausen, M., Meinshausen, N., Hare, W., Raper, S. C. B., Frieler, K., Knutti, R., Frame, D. J., and Allen, M. R.: Greenhouse-gas emission targets for limiting global warming to 2 °C, Nature, 458, 1158–1162, https://doi.org/10.1038/nature08017, 2009.

Metzner, D., Kutterolf, S., Toohey, M., Timmreck, C., Niemeier, U., Freundt, A., and Krüger, K.: Radiative forcing and climate impact resulting from SO2 injections based on a 200,000-year record of Plinian eruptions along the Central American Volcanic Arc, Int. J. Earth Sci., 103, 2063–2079, https://doi.org/10.1007/s00531-012-0814-z, 2014.

Middleton, N. J. and Thomas, D. S. G.: UNEP: World atlas of desertification, 1st edition, Edward Arnold Publishers Ltd, Sevenoaks, UK, 1992.

Mills, M. J., Richter, J. H., Tilmes, S., Kravitz, B., MacMartin, D. G., Glanville, A. A., Tribbia, J. J., Lamarque, J.-F., Vitt, F., Schmidt, A., Gettelman, A., Hannay, C., Bacmeister, J. T., and Kinnison, D. E.: Radiative and Chemical Response to Interactive Stratospheric Sulfate Aerosols in Fully Coupled CESM1(WACCM), J. Geophys. Res.-Atmos., 122, 13061–13078, https://doi.org/10.1002/2017JD027006, 2017.

Ming, Y. and Ramaswamy, V.: Nonlinear Climate and Hydrological Responses to Aerosol Effects. J. Clim., 22, 1329–1339, https://doi.org/10.1175/2008JCLI2362.1, 2009.

Mishra, A. K. and Singh, V. P.: A review of drought concepts, J. Hydrol., 391, 202–216, https://doi.org/10.1016/j.jhydrol.2010.07.012, 2010.

Moore, J. C., Rinke, A., Yu, X., Ji, D., Cui, X., Li, Y., Alterskjaer, K., Kristjánsson, J. E., Muri, H., Boucher, O., Huneeus, N., Kravitz, B., Robock, A., Niemeier, U., Schulz, M., Tilmes, S., Watanabe, S., and Yang, S.: Arctic sea ice and atmospheric circulation under the GeoMIP G1 scenario, J. Geophys. Res.-Atmos., 119, 567–583, https://doi.org/10.1002/2013JD021060, 2014.

Mortimore, M., with contributions from Anderson, S., Cotula, L., Davies, J., Faccer, K., Hesse, C., Morton, J., Nyangena, W., Skinner, J., and Wolfangel, C.: Dryland Opportunities: A new paradigm for people, ecosystems and development, IUCN, Gland, Switzerland; IIED, London, UK and UNDP/DDC, Nairobi, Kenya, 86 pp., 2009.

Muri, H., Tjiputra, J., Otterå, O. H., Adakudlu, M., Lauvset, S. K., Grini, A., Schulz, M., Niemeier, U., and Kristjánsson, J. E.: Climate Response to Aerosol Geoengineering: A Multimethod Comparison, J. Clim., 31, 6319–6340, https://doi.org/10.1175/JCLI-D-17-0620.1, 2018.

Niemeier, U. and Tilmes, S.: Sulfur injections for a cooler planet, Science, 357, 246–248, https://doi.org/10.1126/science.aan3317, 2017.

Niemeier, U., Schmidt, H., Alterskjær, K., and Kristjánsson, J. E.: Solar irradiance reduction via climate engineering: Impact of dif-

ferent techniques on the energy balance and the hydrological cycle, J. Geophys. Res.-Atmos., 118, 11905–11917, 2013.

Peters, G. P., Andrew, R. M., Boden, T., Canadell, J. G., Ciais, P., Le Quéré, C., Marland, G., Raupach, M. R., and Wilson, C.: The challenge to keep global warming below 2 °C, Nat. Clim. Chang., 3, 4–6, https://doi.org/10.1038/nclimate1783, 2012.

Pongratz, J., Lobell, D. B., Cao, L., and Caldeira, K.: Crop yields in a geoengineered climate, Nat. Clim. Chang., 2, 101–105, https://doi.org/10.1038/nclimate1373, 2012.

Robock, A., Marquardt, A., Kravitz, B., and Stenchikov, G.: Benefits, risks, and costs of stratospheric geoengineering, Geophys. Res. Lett., 36, L19703, https://doi.org/10.1029/2009GL039209, 2009.

Rodell, M., Houser, P. R., Jambor, U., Gottschalck, J., Mitchell, K., Meng, C.-J., Arsenault, K., Cosgrove, B., Radakovich, J., Bosilovich, M., Entin, J. K., Walker, J. P., Lohmann, D., and Toll, D.: The Global Land Data Assimilation System, B. Am. Meteorol. Soc., 85, 381–394, https://doi.org/10.1175/BAMS-85-3-381, 2004.

Salter, S.: Spray turbines to increase rain by enhanced evaporation from the sea, Tenth Congress of International Maritime Association of the Mediterranean, Crete, May 2002.

Sanderson, B. M., Xu, Y., Tebaldi, C., Wehner, M., O'Neill, B., Jahn, A., Pendergrass, A. G., Lehner, F., Strand, W. G., Lin, L., Knutti, R., and Lamarque, J. F.: Community climate simulations to assess avoided impacts in 1.5 and 2 °C futures, Earth Syst. Dynam., 8, 827–847, https://doi.org/10.5194/esd-8-827-2017, 2017.

Scheff, J. and Frierson, D. M. W.: Scaling Potential Evapotranspiration with Greenhouse Warming, J. Clim., 27, 1539–1558, https://doi.org/10.1175/JCLI-D-13-00233.1, 2014.

Schiermeier, Q.: Increased flood risk linked to global warming, Nature, 470, 316–316, https://doi.org/10.1038/470316a, 2011.

Seager, R., Feldman, J., Lis, N., Ting, M., Williams, A. P., Nakamura, J., Liu, H., and Henderson, N.: Whither the 100th Meridian? The Once and Future Physical and Human Geography of America's Arid–Humid Divide. Part II: The Meridian Moves East, Earth Interact., 22, 1–24, https://doi.org/10.1175/EI-D-17-0012.1, 2018.

Seneviratne, S. I., Phipps, S. J., Pitman, A. J., Hirsch, A. L., Davin, E. L., Donat, M. G., Hirschi, M., Lenton, A., Wilhelm, M., and Kravitz, B.: Land radiative management as contributor to regional-scale climate adaptation and mitigation, Nat. Geosci., 11, 88–96, https://doi.org/10.1038/s41561-017-0057-5, 2018.

Shindell, D., Kuylenstierna, J. C. I., Vignati, E., van Dingenen, R., Amann, M., Klimont, Z., Anenberg, S. C., Muller, N., Janssens-Maenhout, G., Raes, F., Schwartz, J., Faluvegi, G., Pozzoli, L., Kupiainen, K., Hoglund-Isaksson, L., Emberson, L., Streets, D., Ramanathan, V., Hicks, K., Oanh, N. T. K., Milly, G., Williams, M., Demkine, V., and Fowler, D.: Simultaneously Mitigating Near-Term Climate Change and Improving Human Health and Food Security, Science, 335, 183–189, https://doi.org/10.1126/science.1210026, 2012.

Shuttleworth, W. J.: Chapter 4. Evaporation, Handbook of Hydrology, 1st edition, edited by: Maidment, D. R., McGraw-Hill Education, New York, NY, US, 1993.

Simpson, I. R., Tilmes, S., Richter, J. H., Kravitz, B., MacMartin, D. G., Mills, M. J., Fasullo, J. T., and Pendergrass, A. G.: The Regional Hydroclimate Response to Stratospheric Sulfate Geoengineering and the Role of Stratospheric Heating, J. Geophys. Res.-Atmos., 124, 12587–12616, https://doi.org/10.1029/2019JD031093, 2019.

Stratospheric Aerosol Geoengineering Large Ensemble Project – GLENS: available at: http://www.cesm.ucar.edu/projects/community-projects/GLENS/, last access: 29 July 2020.

Swann, A. L. S.: Plants and Drought in a Changing Climate, Curr. Clim. Change Rep., 4, 192–201, https://doi.org/10.1007/s40641-018-0097-y, 2018.

Tilmes, S., Fasullo, J., Lamarque, J. F., Marsh, D. R., Mills, M., Alterskjær, K., Muri, H., Kristjánsson, J. E., Boucher, O., Schulz, M., Cole, J. N. S., Curry, C. L., Jones, A., Haywood, J., Irvine, P. J., Ji, D., Moore, J. C., Karam, D. B., Kravitz, B., Rasch, P. J., Singh, B., Yoon, J. H., Niemeier, U., Schmidt, H., Robock, A., Yang, S., and Watanabe, S.: The hydrological impact of geoengineering in the Geoengineering Model Intercomparison Project (GeoMIP), J. Geophys. Res.-Atmos., 118, 11036–11058, https://doi.org/10.1002/jgrd.50868, 2013.

Tilmes, S., Sanderson, B. M., and O'Neill, B. C.: Climate impacts of geoengineering in a delayed mitigation scenario, Geophys. Res. Lett., 43, 8222–8229, https://doi.org/10.1002/2016GL070122, 2016.

Tilmes, S., Richter, J. H., Mills, M. J., Kravitz, B., MacMartin, D. G., Vitt, F., Tribbia, J. J., and Lamarque, J.-F.: Sensitivity of Aerosol Distribution and Climate Response to Stratospheric SO_2 Injection Locations, J. Geophys. Res.-Atmos., 122, 12591–12615, https://doi.org/10.1002/2017JD026888, 2017.

Tilmes, S., Richter, J. H., Kravitz, B., MacMartin, D. G., Mills, M. J., Simpson, I. R., Glanville, A. S., Fasullo, J. T., Phillips, A. S., Lamarque, J.-F., Tribbia, J., Edwards, J., Mickelson, S., and Ghosh, S.: CESM1(WACCM) Stratospheric Aerosol Geoengineering Large Ensemble Project, B. Am. Meteorol. Soc., 99, 2361–2371, https://doi.org/10.1175/BAMS-D-17-0267.1, 2018.

UNCCD (United Nations Convention to Combat Desertification): Elaboration of An International Convention to Combat Desertification in Countries Experiencing Serious Drought and/or Desertification, Particularly in Africa, UN Doc. A/A C. 241/27, 33 I.L.M. 1328, United Nations, 58 pp., 1994.

Vaughan, N. E. and Lenton, T. M.: A review of climate geoengineering proposals, Clim. Change, 109, 745–790, https://doi.org/10.1007/s10584-011-0027-7, 2011.

Victor, D. G., Zaelke, D., and Ramanathan, V.: Soot and short-lived pollutants provide political opportunity, Nat. Clim. Chang., 5, 796–798, https://doi.org/10.1038/nclimate2703, 2015.

Wang, Z., Lin, L., Yang, M., Xu, Y., and Li, J.: Disentangling fast and slow responses of the East Asian summer monsoon to reflecting and absorbing aerosol forcings, Atmos. Chem. Phys., 17, 11075–11088, https://doi.org/10.5194/acp-17-11075-2017, 2017a.

Wang, Z., Lin, L., Zhang, X., Zhang, H., Liu, L., and Xu, Y.: Scenario dependence of future changes in climate extremes under 1.5 °C and 2 °C global warming, Sci. Rep., 7, 46432, https://doi.org/10.1038/srep46432, 2017b.

Wigley, T. M. L.: A Combined Mitigation/Geoengineering Approach to Climate Stabilization, Science, 314, 452–454, https://doi.org/10.1126/science.1131728, 2006.

Xu, Y. and Ramanathan, V.: Well below 2 °C: Mitigation strategies for avoiding dangerous to catastrophic climate changes, P. Natl. Acad. Sci. USA, 114, 10315–10323, https://doi.org/10.1073/pnas.1618481114, 2017.